Article

Developmental Cell

Gli1+ Periodontium Stem Cells Are Regulated by Osteocytes and Occlusal Force

Highlights

- Perivascular Gli1+ cells are stem cells (PDLSCs) for the periodontal tissue
- Wnt signal is essential for PDLSC activity
- Sclerostin secreted from bones represses Wnt and PDLSC activities
- Biting force regulates PDLSC activity by modulating sclerostin level

Authors

Yi Men, Yuhong Wang, Yating Yi, ..., Woo-Ping Ge, Jian Q. Feng, Hu Zhao

Correspondence

huzhao@tamu.edu or huzhaolab@gmail.com

In Brief

Teeth are suspended within alveolar bone through a fibrous tissue called periodontal ligament and are subject to biting force during mastication. Men et al. identify Gli1+ cells as periodontal stem cells (PDLSCs). PDLSCs surround the neurovascular bundle and are regulated by osteocytes and biting force.

Men et al., 2020, Developmental Cell *54*, 639–654
September 14, 2020
https://doi.org/10.1016/j.devcel.2020.06.006

CellPress

Developmental Cell

CellPress

Article

Gli1+ Periodontium Stem Cells Are Regulated by Osteocytes and Occlusal Force

Yi Men,[1,2,7] Yuhong Wang,[1,2,7] Yating Yi,[1] Dian Jing,[1] Wenjing Luo,[3] Bo Shen,[4] William Stenberg,[1] Yang Chai,[5] Woo-Ping Ge,[6] Jian Q. Feng,[3] and Hu Zhao[1,8,*]

[1]Department of Comprehensive Dentistry, College of Dentistry, Texas A&M University, Dallas, TX 75246, USA
[2]West China School of Stomatology, Sichuan University, Chengdu, Sichuan 610041, China
[3]Department of Biomedical Sciences, College of Dentistry, Texas A&M University, Dallas, TX 75246, USA
[4]Children's Research Institute, UT Southwestern Medical Center Dallas, TX 75235, USA
[5]Center for Craniofacial Molecular Biology, University of Southern California, Herman Ostrow School of Dentistry, Los Angeles, CA 90089, USA
[6]Chinese Institute for Brain Research, Beijing 102206, China
[7]These authors contributed equally
[8]Lead Contact
*Correspondence: huzhao@tamu.edu or huzhaolab@gmail.com
https://doi.org/10.1016/j.devcel.2020.06.006

SUMMARY

Teeth are attached to alveolar bone by the periodontal ligament (PDL), which contains stem cells supporting tissue turnover. Here, we identified Gli1+ cells in adult mouse molar PDL as multi-potential stem cells (PDLSCs) giving rise to PDL, alveolar bone, and cementum. They support periodontium tissue turnover and injury repair. Gli1+ PDLSCs are surrounding the neurovascular bundle and more enriched in the apical region. Canonical Wnt signaling is essential for their activation. Alveolar bone osteocytes negatively regulate Gli1+ PDLSCs activity through sclerostin, a Wnt inhibitor. Blockage of sclerostin accelerates the PDLSCs lineage contribution rate *in vivo*. Sclerostin expression is modulated by physiological occlusal force. Removal of occlusal force upregulates sclerostin and inhibits PDLSCs activation. In summary, Gli1+ cells are the multi-potential PDLSCs *in vivo*. Osteocytes provide negative feedback to PDLSCs and inhibit their activities through sclerostin. Physiological occlusal force indirectly regulates PDLSCs activities by fine-tuning this feedback loop.

INTRODUCTION

Teeth are subject to cyclic occlusal force during activities such as mastication throughout life. They are anchored to the supporting alveolar bone through a highly flexible and strong fibrous tissue called the periodontal ligament (PDL). The PDL fibers insert into the cementum on the tooth surface and into the periosteum on the alveolar bone surface to form a functional unit called the periodontium (Ten Cate, 1997). The three components of the periodontium are all derived from cranial neural crest cells during development (Chai et al., 2000). Adult periodontium tissue undergoes constant turnover (Lin et al., 2014; Ivanovski et al., 2006). *In vitro* studies have identified the presence of periodontal stem cells (PDLSCs) that possess multipotential differentiation capability *in vitro* (Seo et al., 2004). αSMA+ (α smooth muscle actin) was proposed to be a marker of PDLSCs *in vivo* (Roguljic et al., 2013). However, lineage tracing experiments showed αSMA+ cells make minor contribution during periodontium injury repair and even less during homeostasis. *Axin2* was also proposed as the marker for PDL progenitors (Zhang et al., 2019; Xu et al., 2019). However, *Axin2* is also widely expressed by odontoblast and osteoblast and, therefore, is not a specific marker (Lim et al., 2014). PTHrP+ (parathyroid hormone related protein) cells support tooth root development but contribute little to the adult periodontium (Ono et al., 2016; Takahashi et al., 2019). *In vivo* identification of adult periodontal multi-potential PDLSCs, thus, remains elusive.

Wnt plays critical roles during tooth initiation and morphogenesis, as well as terminal differentiation (Järvinen et al., 2018; Liu et al., 2008; Lan et al., 2014; Balic and Thesleff, 2015). Wnt signaling is essential for stem cells in various organs including the lung, liver, skin, and intestine (Farin et al., 2016; Degirmenci et al., 2018; Lee et al., 2017; Wang et al., 2015) . It is also essential for adult stem cells in tooth, long bone, and calvarial bones. Blockage of Wnt pathway causes numerous abnormalities in stem cell activation, proliferation, and differentiation (An et al., 2018; Maruyama et al., 2016; Shi et al., 2017). Under physiological conditions, Wnt activity was rarely regulated in an on or off fashion. Instead, level of Wnt activity was modulated by various pathways or inhibitor. Indian hedgehog (Ihh) inhibits intestine stem cell activities by inhibiting Wnt signaling pathway (Kosinski et al., 2010). DKK1, DKK3, and WIF1 promote terminal differentiation of epidermal stem cells by downregulating Wnt signaling (Lim et al., 2013). For stem cells of bones or teeth, much less was known about how Wnt activity is modulated within the stem cell niche.

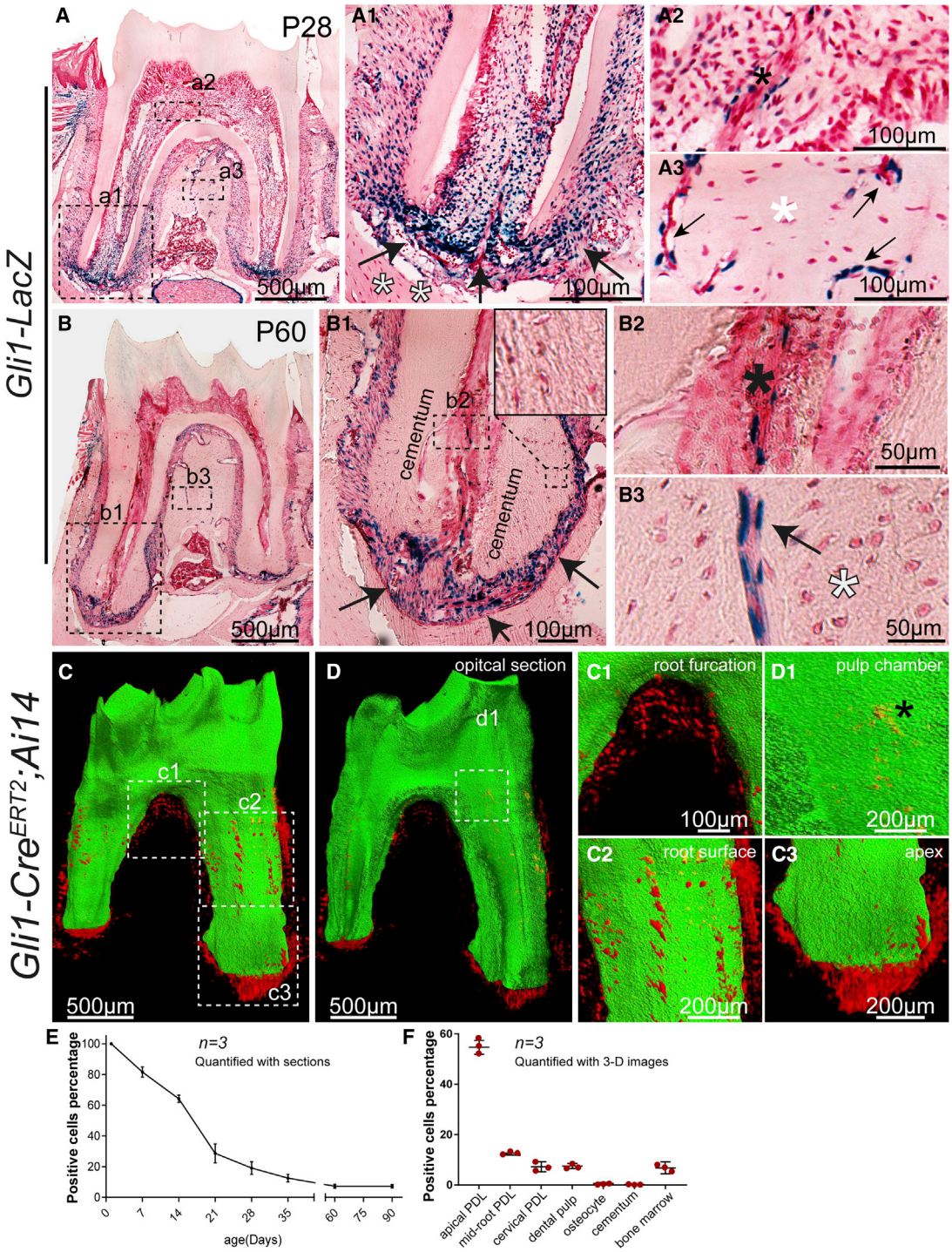

Figure 1. Majority of Gli1+ Cells Are Distributed within the PDL Near the Tooth Apical Region but Are Absent from Alveolar Bone, Dentin, Cementum, and Coronal Pulp Tissue within the Periodontium of Adult Mouse Molars

(A) LacZ staining of the lower 1st molar of a *Gli1-LacZ* mouse at P28. Boxed regions are enlarged in (A1), (A2), and (A3), respectively.

(B) LacZ staining of the lower 1st molar of a *Gli1-LacZ* mouse at P60. Boxed areas are enlarged in B1, B2, and B3, respectively. Arrows indicate Gli1+ cells within the PDL or bone marrow. Gli1+ cells are absent from the cementum (B1 and B1 insert), dentin (A1 and B1), or alveolar bone osteocyte (white asterisks in A3 and B3). Black asterisks indicate sparse Gli1+ cells within the dental pulp.

(C) Adult *Gli1-Cre^{ERT2};Ai14* mice were induced with tamoxifen to label Gli1+ cells. Mandibles were processed for tissue clearing and 3D imaging. Boxed regions are enlarged in (C1), (C2), and (C3), respectively.

(D) An optical section was acquired to show sparse Gli1+ cells within the pulp (black asterisk). Boxed region is enlarged in D1.

(legend continued on next page)

Mechanical force plays key roles in embryonic development, as well as in tissue healing and repair. Extra- and intra-cellular molecules, membrane proteins and cytoskeletal components, and signaling pathways have been shown to play critical roles on determining how somatic stem cells sense and transmit mechanical signals, including N-cadherin, YAP/TAZ, Wnt, Kindlin-2, RAP2 (Ras-related GTPase 2), SWI/SNI (SWItch/Sucrose Non-Fermentable), etc. (Chang et al., 2018; Meng et al., 2018; Cosgrove et al., 2016). Hard tissue organs including bone, teeth, and tendon are subject to cyclic mechanical forces. Most studies investigated mechano-regulation of mesenchymal stem cells on the culture dish (Cosgrove et al., 2016; Guo et al., 2018; Kurpinski et al., 2006). Little is known on how stem cells of bones or teeth respond to the mechanical force *in vivo*.

In this study, we identified Gli1+ cells within the PDL as the multipotential stem cells of adult mouse periodontium (PDLSCs). They are undifferentiated cells that surround the neurovascular bundle (NVB) and give rise to alveolar bone, cementum, and PDL. Canonical Wnt signaling is critical for their activation and maintenance. Sclerostin secreted from the alveolar bone osteocytes is a Wnt inhibitor and negatively regulates Gli1+ cells activity. Occlusal force is essential for Gli1+ cells activation. Unloading of teeth attenuates Gli1+ PDLSCs and Wnt activities. Blockage of sclerostin eliminates stem cells responsiveness to occlusal force. Our study identified a stem cells niche mechanism in which osteocytes provide feedback to stem cells and regulate their activities. Physiological occlusal force regulates stem cells by fine-tuning this feedback loop.

RESULTS

Gli1+ Cells Are Mainly Located within the Apical PDL Space of Adult Molars

Gli1+ cells have been identified as the stem cells for the mouse incisor, craniofacial bones, and long bone (Shi et al., 2017; Zhao et al., 2015). Gli1+ cells within the apical dental pulp were also shown to support root development regulated by Bmp signaling pathway (Feng et al., 2017). We hypothesized that Gli1+ cells might also be the stem cells of adult mouse periodontium. To characterize the Gli1+ cells within the periodontium, we generated *Gli1-LacZ* mice. With LacZ staining, Gli1+ cells were detected throughout the entire tooth germ on post-natal day 1 (P1), P7, and P14 (Figures S1A–S1C). After P21, Gli1+ cells were gradually restricted to the apical dental pulp near the root orifice (Figure S1D). At P28, Gli1+ cells were mainly located within the PDL space of the apical region. Less Gli1+ cells were detected in the pulp, alveolar bone marrow space, or periodontal tissue of the non-apical region (Figures 1A1 and 1A2). No Gli1+ expression was detected within terminally differentiated osteocytes, odontoblast, or cementoblasts (Figures 1A1 and 1A2). A similar distribution pattern was also detected in molar PDL at P60 (Figures 1B–1B2). Quantification indicated that the ratio of Gli1+ cells within the entire periodontium reduced from 100% at P1 to ~20% at P21 and was maintained at ~5% from P30 to P90 (Figure 1E).

To visualize distribution of PDL Gli1+ cells in three dimensions, *Gli1-Cre^{ERT2};Ai14* mice of P60 old were induced with tamoxifen and processed following the PEG associated solvent system (PEGASOS) tissue clearing method (Jing et al., 2018). Second harmonic generation (SHG) signal was used to display the type I collagen-enriched hard tissue (Acar et al., 2015). We were able to visualize and quantify the spatial distribution pattern of Gli1+ cells within the periodontium (Figures 1C and 1D). Quantification indicated that ~60% of Gli1+ cells were located within the apical PDL space, ~18% in the middle PDL space, ~10% in the cervical PDL space, ~10% in the alveolar bone marrow space or in the dental pulp (mostly root pulp). No Gli1+ cells were detected in cementum or alveolar bone osteocyte. (Figure 1F).

Gli1+ Cells *In Vivo* Are Negative for Periodontium Differentiation and Classical Stromal Stem Cells Markers

To examine the differentiation status of Gli1+ cells, we induced adult *Gli1-Cre^{ERT2};Ai14* mice to label Gli1+ cells (Shi et al., 2017; Zhao et al., 2015; Schneider et al., 2017). Immunofluorescent staining was then performed. Periostin is a PDL-specific marker (Horiuchi et al., 1999). Its expression was detected in nearly the entire PDL except the apical region and Gli1+ cells (Figures 2A and 2A1). Sp7 and type 1 collagen are known to be expressed by osteoblasts and osteocytes, respectively. Their expression does not colocalize with Gli1+ cells (Figures 2B, 2B1, 2C, and 2C1). Strong CD44 expression was detected in the entire PDL, with the exception of the apical region and Gli1+ cells (Figures S1E and S1E1). CD73 expression was detected in the gingiva epithelium, but not in the periodontium (Figures S1F and S1H). CD146 expression was detected surrounding vasculature throughout the entire periodontium but rarely colocalized with Gli1+ cells (Figures S1G and S1G1).

Gli1+ Cells Surround the NVB of the PDL

Gli1+ cells within the mouse incisor were shown to surround the NVB (Zhao et al., 2014). Utilizing the PEGASOS clearing method followed by 3D imaging, we investigated the neurovascular organization of the PDL tissue. We cleared the mandibles from adult *Cdh5-Cre^{ERT2};Ai14* mice after induction with tamoxifen (Jeong et al., 2017). Deep imaging revealed enriched vasculature within the pulp chamber and PDL space (Figures 2D and 2D1). Using the *Synapsin1-Cre;Ai14* mouse model, we also visualized enriched nerve fibers within the PDL space and pulp chamber (Figure 2E). Importantly, both vasculature and nerves were more enriched in the apical region due to the convergence of the pulp and PDL neurovascular structures (Figures 2D1 and 2E). To investigate whether Gli1+ cells in the periodontium were also located surrounding the NVB, β3-Tubulin and GS-IB4 staining were performed on horizontal cross-sections of molars to show the nerves and vasculature, respectively. All Gli1+ cells were exclusively surrounding the vasculature (Figures 2F and 2G) and nerve bundles (Figure 2H).

(E) Percentages of Gli1+ cells within the PDL at different ages were quantified based on sections.
(F) Percentage of Gli1+ cells in different regions of an adult molar were quantified based on 3D imaging. The cell number was estimated from the volume assuming a similar cell size. n = 3. Results are displayed as mean ± SD. See also Figure S1.

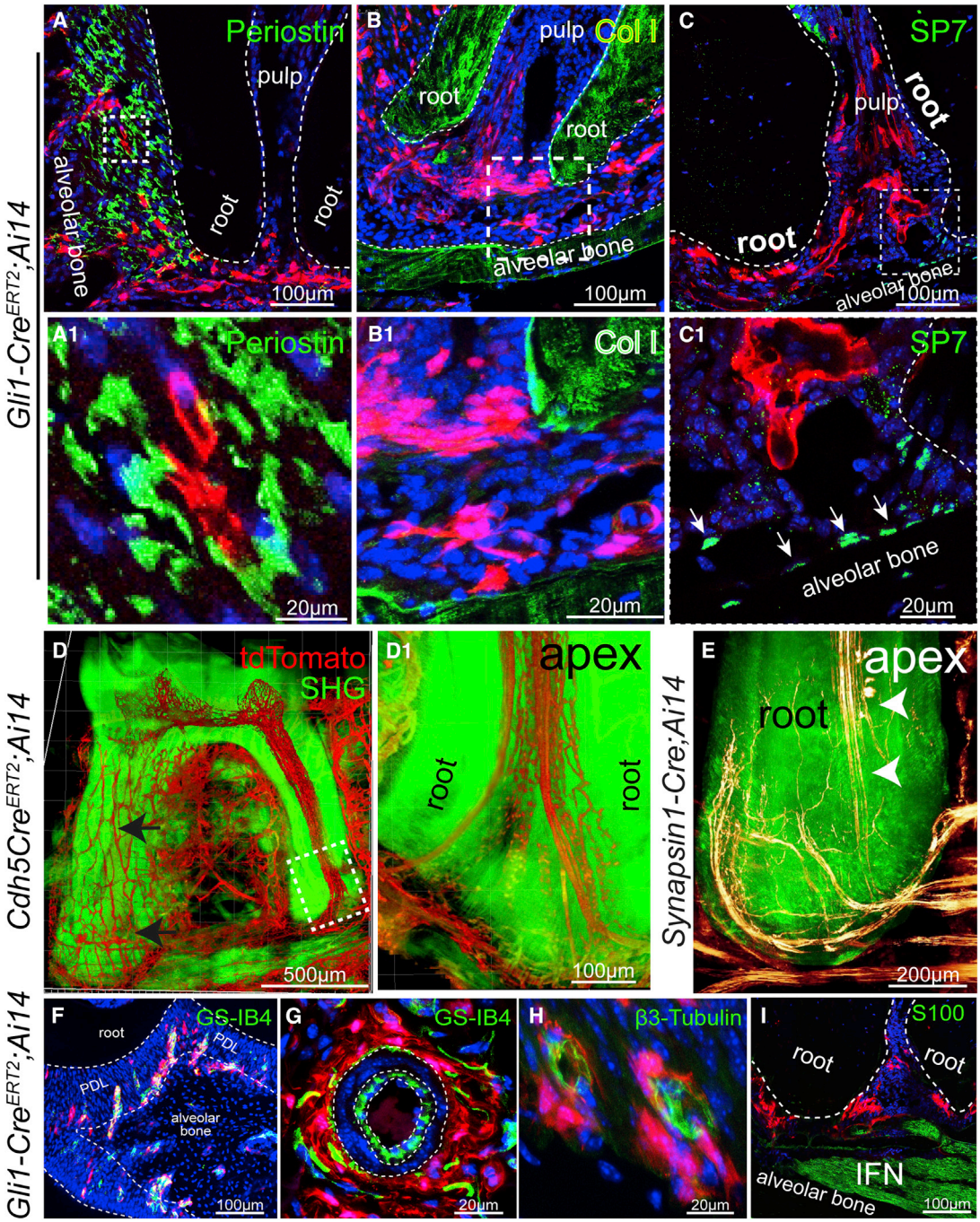

Figure 2. Gli1+ Cells Are Negative for Differentiation Markers and Surround the NVB

(A–C) Adult *Gli1-Cre^{ERT2};Ai14* mice were induced with tamoxifen. Immunofluorescent staining was performed with antibodies against periostin (A), type 1 collagen (B), and Sp7 (C). Boxed regions were enlarged or re-imaged in (A1), (B1), and (C1). Arrows in (C1) indicate *Sp7*+ cells.

(D) Vascular network within the PDL space. Adult *Cdh5-Cre^{ERT2};Ai14* mice were induced with tamoxifen. PEGASOS tissue clearing was performed for 3D images to reveal vascular network within the PDL space (arrows in D). Image stack at the boxed region is resliced in (D1) to show the convergence of blood vessels in the apex region.

(E) Neural network within the PDL space. *Synapsin1-Cre;Ai14* mice molars were cleared for 3D images to display nerves within the root canal (arrowheads) and apical PDL space (arrows).

(F) GS-IB4 staining to reveal the association of Gli1+ cells with blood vessels.

(G) Higher magnification image to show peri-vascular distribution of Gli1+ cells.

(H) β3-tubulin staining to reveal association of Gli1+ cells with nerve fibers.

(I) Gli1+ cells are negative for S100 expression. IFN, inferior alveolar nerve. See also Figure S1.

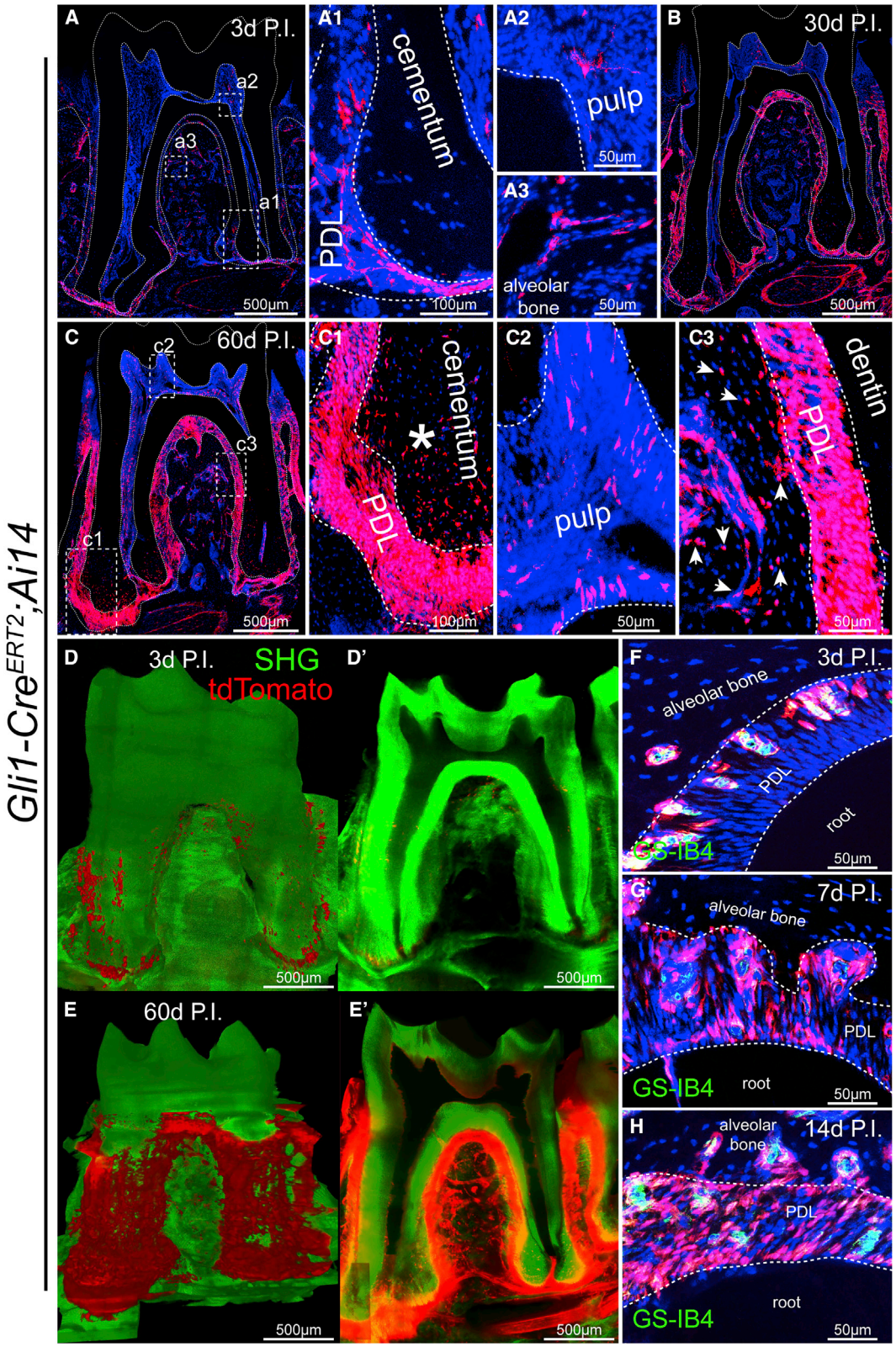

(legend on next page)

The inferior alveolar nerve (IAN), which innervate both lower incisors and molars, was known to secret sonic hedgehog (SHH) and regulate Gli1+ incisor stem cells (Zhao et al., 2014). Using induced adult *Shh-Cre^{ERT2};Ai14* mice, we confirmed *Shh* expression within the trigeminal ganglion, IAN, and nerve axons near the molar root apical region (Figures S1H–S1J). As a positive control, strong Shh expression was also detected in the incisor epithelium (Figure S1K).

Gli1+ Cells Contribute to Periodontium Tissue Turnover by Migrating out of the NVB Niche

To trace the fate of Gli1+ cells *in vivo*, we induced adult *Gli1-Cre^{ERT2};Ai14* mice. On day 3 after induction, positive cells were detected mainly in the apical PDL but are absent from the cementum or alveolar bone osteocyte, which is consistent with the lacZ staining pattern (Figures 3A–3A3, 3E, and S2K). A few Gli1+ cells were also detected within the alveolar bone marrow space and dental pulp (Figures 3A2 and 3A3). Thirty days after induction, Gli1+ cells contributed to 60% of the PDL, 30% of cementoblast, and 5% of alveolar bone osteocytes (Figures 3B and 3K). Sixty days after induction, Gli1+ cells contributed to 95% of PDL, 55% of cementoblast, 10% of dental pulp, and 10% of alveolar bone osteocytes (Figures 3C–3C3 and S2J). Most of the labeled osteocytes are located within the alveolar bone proper, which directly contacts the PDL (Figure 3C3 Eight months after induction, Gli1+ cells contributed to 99% of PDL, 93% of cementoblast, and 85% of alveolar bone osteocyte (Figures S2I– S2I2 and S2J). 3D imaging based on PEGASOS-cleared molars collected 3 days (Figures 3D and 3D′) or 60 days (Figures 3E and 3E′) after induction also showed similar contribution patterns. Contribution of Gli1+ cell toward dental pulp was still around 10% even at 8 months after induction (Figures S2I and S2J). Molars were also collected at 3, 7, or 14 days after induction, and Griffonia simplicifolia isolectin B4 (GS-IB4) staining was performed on horizontal root sections to label vasculature. TdTomato+ cells were detected in the peri-vascular regions and gradually populated the entire PDL space (Figures 3F–3H).

We also titrated down the tamoxifen induction dosage. With the reduced induction dosages, much less Gli1+ cells were observed within the PDL space (Figures S2A–S2D). 1/128 dosage tamoxifen was injected once to adult *Gli1-Cre^{ERT2};Ai14* mice for *in vivo* clonal assay. Individual cells could be identified on day 3 after induction (Figure S2E). On day 14, isolated clones could be identified within the PDL space (Figure S2F). On day 35 after induction, individual clones were identified including both differentiated osteocyte and cementoblast (Figures S2G and S2H–S2H2).

To investigate whether the Gli1+ population persists, *Gli1-Cre^{ERT2};Ai14* mice at 6 months of age were induced with tamoxifen. On day 7 after induction, sparse Gli1+ cells were detected within the PDL space (Figure S2K). On day 60 after induction, nearly the entire PDL and cementum were labeled (Figures S2L and S2L1). A small portion of alveolar bone osteocytes were also labeled (Figure S2L2).

Collectively, our lineage tracing experiments indicated that Gli1+ cells are multipotential PDLSCs contributing to the periodontium tissue turnover *in vivo*.

Dynamics of Gli1+ Cells and Their Contribution to Injury Repair of the Periodontium

We designed a long duration EdU incorporation assay to demonstrate the PDL tissue turnover. EdU assays of 24, 48, 96 h, or 1 week all showed enriched EdU+ cells surrounding vasculature and Gli1+ cells (Figures S3A–S3D). Combination of Gli1+ cells lineage tracing and 1-week EdU assay indicated nearly all EdU+ cells (∼95%, n = 4) were derived from Gli1+ cells (Figure S3E). Quantification indicated increasingly more PDL cells or Gli1+ cells were labeled with EdU with longer duration. In the 24-h EdU assay, ∼5% of PDL cells and ∼5% of Gli1+ cells were EdU+. In the 1-week EdU assay, ∼24% of PDL cells and ∼20% of Gli1 cells were EdU+ (Figure S3F). Most dividing cells are negative for Gli1(∼80%) (Figure S3F).

A 24-h EdU assay was performed for induced *Gli1-Cre^{ERT2};Ai14* mice after injury. Comparing with the control side molars (Figure S3G), EdU+ PDL cells and EdU+ Gli1+ cells increased by ∼7-fold in the injured PDL. Ratio of EdU+Gli1− cells/all dividing cells are similar in the injured PDL as in the control side PDL (Figures S3H and S3I).

Injured periodontium completely healed 30 days later (Figure S3J). To test contribution of Gli1+ cells to injury repair, we injured the molar furcation of adult *Gli1-Cre^{ERT2};Ai14* mice. Mice were next induced with tamoxifen. On day 7 after induction, a significant amount of PDL tissue near the furcation area (Figures S3K and S3K1) was labeled. Lineage tracing assays indicated that, on the injury side, nearly the entire PDL and a large portion of osteocytes in the furcation area were labeled by tdTomato (Figures S3L and S3L1, arrows), indicating their derivation from Gli1+ cells. In contrast, far fewer PDL or osteocytes on the non-injury side were labeled on day 30 after induction (Figures S3M and S3M1).

These results indicated that most dividing cells are surrounding vasculature and Gli1+ cells. Injury activated Gli1+ cells to support tissue regeneration.

Figure 3. Gli1+ Cells Migrate out of the Perivascular Niche to Give Rise to the Periodontium during the Physiological Turnover of Adult Mouse Molars

Adult *Gli1-Cre^{ERT2};Ai14* mice were induced with tamoxifen.

(A) Section of the lower 1st molar on day 3 after induction. Boxed regions are enlarged in (A1), (A2), and (A3), respectively.

(B) Section of the lower 1st molar on day 30 after induction.

(C) Section of the lower 1st molar on day 60 after induction. Boxed regions are enlarged in (C1), (C2), (C3), respectively. Asterisks indicate positively labeled cementoblasts, indicating their derivation from Gli1+ cells (C1). Arrows indicate positively labeled alveolar bone osteocytes (C3).

(D and E) Mandibles were harvested on day 3 (D) or 60 (E) after induction for tissue clearing and 3D imaging. Optical sections are displayed in d′ and e′, respectively.

(F–H) GS-IB4 staining was performed on horizontal frozen sections of middle roots harvested on day 3 (F), 7 (G), or 14 (H) after tamoxifen induction. Dotted lines outline root and alveolar bone. P.I., post-induction. See also Figures S2–S4.

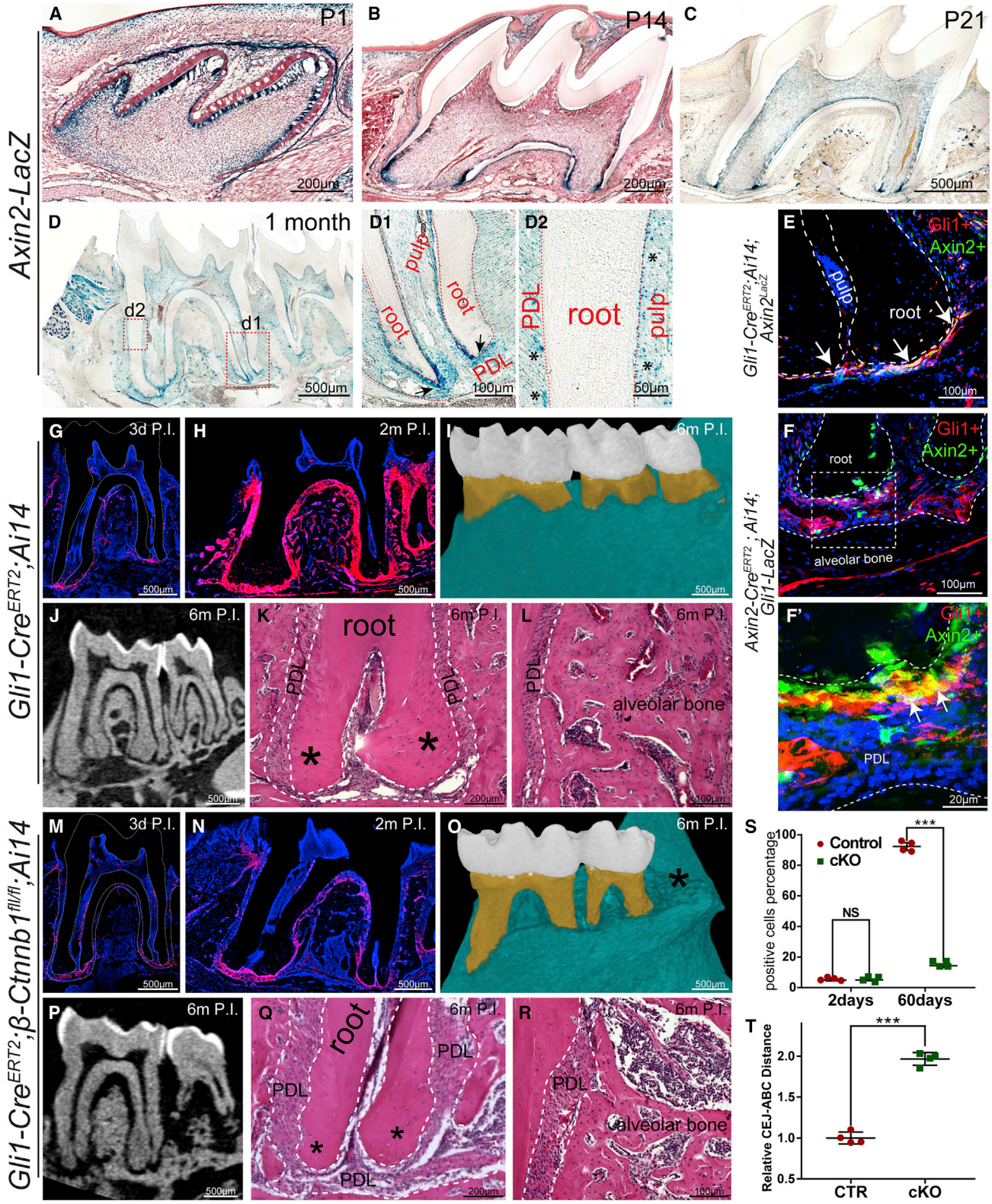

Figure 4. Canonical Wnt Signaling Is Essential for Activation of Gli1+ Cells and Homeostasis of Periodontium Tissue

(A–D) LacZ staining of molars of *Axin2-LacZ* mice at ages of P1 (A), P14 (B), P21 (C) and P30 (D). Boxed regions in (D) are enlarged in D1 and D2 respectively. Arrows in (D1) indicate *Axin2*+ cells in the apical regions. Asterisks in (D2) indicate *Axin2*+ cells at the root surface and pulp.

(legend continued on next page)

Gli1+ PDLSCs Express Stromal Cell Markers and Undergo Multilineage Differentiation *In Vitro*

We isolated PDLSCs from the molar root surface of adult *Gli1-Cre^{ERT2};Ai14* mice on day 3 after a full dosage induction. Two weeks after plating, all visible cells on the dish were positive for tdTomato indicating their derivation from Gli1+ cells (Figure S4A). We performed immunohistochemical staining of cultured cells. Hematopoietic and endothelial markers including CD31 and CD34 were not detectable in the culture (Figures S4B and S4C). Although Gli1+ cells *in vivo* do not express stromal cell markers, cultured PDLSCs highly express CD44, CD146, and CD73 (Figures S4D–S4F). They also highly express Sp7, but not αSMA, nestin, or periostin (Figures S4G–S4J). Quantified results confirmed our results (Figure S4K). Expression profile difference between *in vivo* and *in vitro* is because the culture condition changes cell surface marker expression, and cells acquire markers that are characteristic of adherent fibroblastic cells.

Three weeks after plating, cultured PDL cells reached confluence and were passaged for differentiation assay using osteogenic, chondrogenic, or adipogenic culture medium. Alizarin red and Alcian blue staining confirmed osteogenic and chondrogenic differentiation (Figures S4L and S4M). Interestingly, little adipogenic differentiation was observed (Figure S4N). *In vitro* osteogenic or chondrogenic differentiation of cultured PDL cells was also confirmed with real-time PCR experiments, which indicated significantly increased expression of osteogenic or chondrogenic genes including *osteopontin*, *Alkaline phosphatase*, *type I collagen*, *Aggrecan*, *Sox9*, and *type 2 collagen* (Figure S4O). These experiments suggest Gli1+ cells possess osteogenic and chondrogenic differentiation potential *in vitro*.

αSMA, LepR, NG2, and Pdgfrα Are Not Efficient Markers for Periodontium Stem Cells

αSMA+ cells were proposed as periodontium stem cells (Roguljic et al., 2013). LepR+, NG2+, or Pdgfrα+ cells are stem cells of long bone, incisor, or adipose tissue respectively (Zhou et al., 2014; Miwa and Era, 2018; Pang et al., 2016). We tested the contribution of these cell populations to the periodontium.

Adult *NG2-Cre^{ERT};Ai14* mice were induced with tamoxifen. On day 3 after induction, cells in the PDL (1%) and pulp tissue (15%) were sparsely labeled whereas nearly all alveolar bone osteocytes (89%) were labeled, suggesting endogenous expression of NG2 by osteocytes (Figures S5A–S5A3). On day 30 after induction, 90% of alveolar bone osteocytes, 18% of dental pulp, and 2% of PDL tissue were positively labeled (Figures S5B–S5B3 and S6J). Adult *Pdgfrα-Cre^{ER};Ai14* mice were induced with tamoxifen. On day 3 after induction, 75% of the pulp cells, 0.17% of osteocytes, and 0.5% of PDL cells were labeled (Figures S5C–S5C3 and S6J). On day 60, 85% of the dental pulp, 16% of alveolar bone osteocyte, and 2% of PDL cells were labeled (Figures S5D–S5D3 and S6J). These results indicate that NG2 and Pdgfrα are neither specific nor efficient markers for labeling periodontium stem cells. NG2 or Pdgfrα antibody staining were performed on molars of induced adult *Gli1-Cre^{ERT2};Ai14* mice. On day 2 after induction, Gli1+ cells were seen not overlapping with NG2 or Pdgfrα cells (Figures S5E and S5G). On day 60, all NG2 or Pdgfrα cells were positively labeled, indicating their derivation from Gli1+ cells (Figures S5F and S5H).

Adult *αSMA-Cre^{ERT2}* mice were induced with tamoxifen. On day 3 after induction, ~3% PDL cells were detected exclusively surrounding vasculature, where they co-localized with smooth muscle cells identified with αSMA antibody (Figures S6A, S6B, and S6J). On day 60, less than 5% of PDL cells were detected within the PDL, suggesting a minor contribution to the periodontium during physiological turnover (Figures S6C–S6C2 and S6J). In adult *LepR-Cre;Ai14* mice (4 weeks) periodontium, 3% of the PDL cells, 0.5% of alveolar bone osteocytes, and 5% of dental pulp cells were labeled (Figures S6D–S6D3). In *LepR-Cre;Ai14* mice at 6 months of age, almost same amount of positive cells were detected within the PDL (7%), alveolar bone (2%), or dental pulp (4%) (Figures S6E–S6E2 and S6J). GS-IB4 staining indicated that the majority of LepR+ cells were surrounding vasculature (Figure S6E3). αSMA and LepR antibody staining were performed on molars of tamoxifen-induced adult *Gli1-Cre^{ERT2};Ai14* mice. On day 2 after tamoxifen induction, Gli1+ cells were seen surrounding, but not overlapping with, αSMA+ or LepR+ cells (Figure S6F and S6H). On day 60 after induction, all αSMA+ and LepR+ cells were positively labeled, indicating their derivation from Gli1+ cells (Figures S6G and S6I).

These results indicated that αSMA+, LepR+, NG2+, or Pdgfrα+ cells have no major contribution to the periodontium tissue and are derived from Gli1+ cells.

Canonical Wnt Signaling Is Essential for Activation of Gli1+ Cells and Periodontium Tissue Maintenance

Canonical Wnt signaling was known to be critical for stem cells populations within other organs (An et al., 2018; Maruyama et al., 2016; Shi et al., 2017). We would like to find out if it is also essential for Gli1+ PDLSCs. To analyze the Wnt activity within the periodontium, we performed lacZ staining of *Axin2-LacZ* mice molars from different developmental stages. At P1, *Axin2* expression was widely detected in nearly the entire dental follicle and epithelium (Figure 4A). From P7 to P21, *Axin2* expression was gradually restricted to the apical area of the tooth germ (Figures 4B and 4C). At one month, *Axin2* expression was detected within the odontoblasts, osteoblasts, and cementoblasts, which is consistent with previous studies (Yin et al., 2015) (Figures 4D and 4D2). Interestingly, strong *Axin2* expression was also detected in the apical region, close to where Gli1+ cells are located (Figure 4D1). β-gal antibody staining of adult

(E and F) Adult *Gli1-Cre^{ERT2};Ai14;Axin2-LacZ* (E) or *Axin2-Cre^{ERT2};Ai14;Gli1-LacZ* (F) mice were induced with tamoxifen. β-Gal antibody immunofluorescent staining was performed to demonstrate expression of *Axin2* by Gli1+ cells. Boxed region in (F) was re-imaged to show Gli1+ cells expressing *Axin2*+ (arrows in F′). (G–L) Adult *Gli1-Cre^{ERT2};Ai14* (Ctrl) mice were induced with tamoxifen and euthanized on day 3 (G), day 60 (H) or 6 months (I–L) after induction. Asterisks in (K) indicate cementum. (M–R) Adult *Gli1-Cre^{ERT2};Ai14;Ctnnb1$^{f/f}$* (CKO) mice were induced with tamoxifen and euthanized on day 3 (M), day 60 (N) or 6 months (O–R) after induction. Asterisks in (Q) indicate cementum. (S) Percentages of tdTomato+ cells within ctrl and CKO molar periodontium on day 2 or 60 after induction were quantified. n = 4.

(T) Periodontium tissue loss was quantified by measuring relative Cementum enamel junction-Alveolar bone crest distance (CEJ-ABC distance) in control and CKO molars 60 days after induction. n = 4. Results are displayed as mean ± SD. P.I., post induction. See also Figure S7.

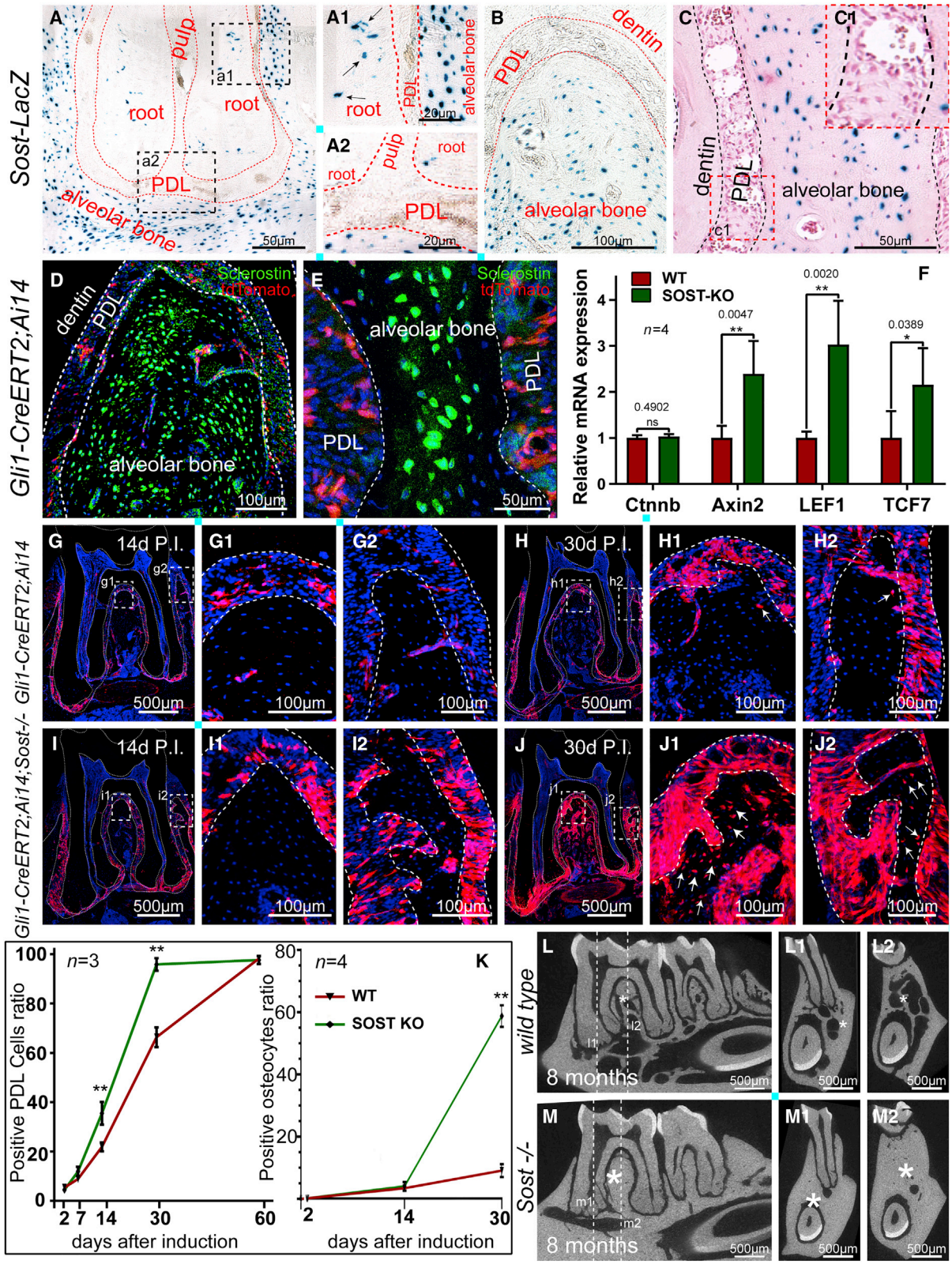

(legend on next page)

Gli1-Cre^{ERT2};Ai14;Axin2-LacZ mice after a brief two-day induction indicated that some Gli1+ cells express *Axin2* (Figure 4F). Colocalization was also confirmed with β-gal antibody staining of induced adult A*xin2-Cre^{ERT2};Ai14;Gli1-LacZ* mice molars (Figures 4F and 4F′). These results suggest the presence of Wnt activity within Gli1+ cells.

We induced adult *Gli1-Cre^{ERT2};Ctnnb1f^{f};Ai14* (β-catenin ICKO [inducible conditional knockout]) mice with tamoxifen. On day 3 after induction, positively labeled Gli1+ cells could be visualized in both *Gli1-Cre^{ERT2};Ai14* (control) and ICKO mice (Figures 4G and 4M). On day 60 after induction, Gli1+ PDLSCs in control mice populated the entire PDL normally (Figure 4H). In contrast, Gli1+ PDLSCs in the ICKO mouse PDL failed to populate the periodontium and were arrested in their original locations, mostly at the apical area (Figure 4N).

Six months after induction, severe periodontal tissue loss was found in the ICKO group. μCT analysis indicated that, compared with the control mice (Figures 4I and 4J), the alveolar bone height and density in the ICKO mice was significantly reduced (Figures 4O and 4P). Over half of the molar root surface was exposed (Figures 4S and 4T). Histological sections also confirmed a severe reduction in the amount of bone and the presence of a wider PDL space in the ICKO mouse periodontium (Figures 4K, 4L, 4Q, and 4R).

To investigate the impact of over-activated Wnt signaling on Gl1+ PDLSCs, we induced adult *Gli1-Cre^{ERT2};Ctnnb1-$^{fl(ex3)/+}$;Ai14* (Exon3 mutant) mice with tamoxifen. On day 2 after induction, 24-h EdU incorporation assay indicated that substantially more proliferating Gli1+ cells were detected within the periodontium of Exon3 mutants compared with control mice (Figures S7A, S7D, and S7G). On day 21 after induction, excessive cementum was detected on the Exon3 mutant root surface (Figures S7B, S7E, and S7H). Histological sections also confirmed excessive cementum formation (Figures S7C and S7F). Fluorescent images indicated that more cells within the PDL of the Exon3 mutant mice (Figures S7K and S7K2) were positively labeled than in control mice (Figures S7J and S7J2) on day 21 after induction. All cementoblasts within the Exon3 mutants (Figure S7K1) were positively labeled, indicating their derivation from Gli1+ cells, whereas few fluorescent cementoblasts were detected in control mice (Figure S7J1). The alveolar bone presented no significant phenotypes in the mutant mice, probably due to the relatively slow turnover rate of this tissue (Figures S7B, S7E, and S7I). Exon3 mutant mice died four weeks after induction, likely due to skin abnormalities.

These results indicated that canonical Wnt signaling is essential for Gli1+ PDLSCs activation and periodontium tissue maintenance. Blockage of Wnt signaling arrested Gli1+ PDLSCs activation. Constitutively activated Wnt signaling over-activated Gli1+ PDLSCs and led to excessive cementum formation.

Sclerostin Secreted by Osteocytes Negatively Regulates Canonical Wnt and Gli1+ Cells Activity within the Periodontium

Sclerostin *(Sost)* is known to be expressed by osteocytes (Delgado-Calle et al., 2017). We performed LacZ staining of *Sost-LacZ* mouse molars. *Sost* expression was detected in alveolar bone osteocytes in the molar apical, furcation, and interdental regions (Figures 5A–5C). *Sost* expression was also detected in cementoblast on the root surface (Figure 5A1). No expression was detected in PDL or dentin (Figures 5A2 and 5C1). Immunofluorescent staining with *Sost* antibody also confirmed specific expression of *Sost* by osteocytes, but not dentin or PDL (Figures 5D and 5E). Gli1+ cells did not express *Sost* (Figures 5D and 5E). Real-time PCR was performed to compare *Wnt* activity levels between *Sost$^{-/-}$* and wild-type mouse periodontium. Expression levels of *Axin2, Tcf7*, and *Lef1* were all significantly upregulated in the periodontium of Sost$^{-/-}$ mice, indicating elevated canonical *Wnt* activity (Figure 5F).

To test the effect of Sost blockage on Gli1+ cells, we induced adult *Gli1-Cre^{ERT2};Ai14;Sost$^{-/-}$* mice *(G;T;Sost$^{-/-}$)* with tamoxifen. On 14 days after induction, more positive cells were detected *in G;T;Sost$^{-/-}$* mouse periodontium than in control mice (Figures 5G–5G2 and 5I–5I2). On day 30 after induction, nearly the entire PDL was labeled with tdTomato in *G;T;Sost$^{-/-}$* mice, whereas only part of the PDL was labeled in the control mice (Figures 5H–5H2 and 5J–5J2). The accelerated PDL contribution rate in *G;T;Sost$^{-/-}$* mice was confirmed by quantification (Figure 5K). Interestingly, although few osteocytes were positive in control mice (Figures 5H1 and 5H2), a lot more positive osteocytes were detected in *G;T;Sost$^{-/-}$* mice alveolar bone, indicating accelerated bone contribution by Gli1+ cells in the absence of sclerostin (Figures 5J1, 5J2, and 5K). In addition, more bone was observed in *Sost$^{-/-}$* mice at eight months of age (Figures 5L–5L2 and 5M–5M2).

Figure 5. Gli1+ PDLSCs are Negatively Regulated by Osteocytes through Sclerostin

(A) LacZ staining of *Sost^{LacZ}* mouse molars to show *Sost* expression surrounding the root. Boxed regions were enlarged to show *Sost*+ cells in the cementoblast (arrows in (A1)) and absence of *Sost* in the PDL (A2).

(B) LacZ staining of *Sost^{LacZ}* mouse molars to show *Sost*+ cells in the furcation region.

(C) LacZ staining on a horizontal section of the root to display *Sost* expression within the alveolar bone. Boxed region was enlarged in (C1).

(D and E) Adult *Gli1-Cre^{ERT2};Ai14* mice were induced with tamoxifen and euthanized on day 3. Immunofluorescent staining with Sclerostin antibody was performed on a longitudinal (D) or horizontal (E) section of the root.

(F) RNA was harvested from periodontium tissue of wild type or *Sost$^{-/-}$* mice. Real-time PCR was performed to analyze gene expression changes with unpaired t test.

(G–J) Adult *Gli1-Cre^{ERT2};Ai14* (H and I) and *Gli1-Cre^{ERT2};Ai14;Sost$^{-/-}$* (J and K) mice were induced with tamoxifen. Mandibles were harvested 2 weeks (G and I) or one month (H and J) after induction. Boxed regions are enlarged in (G1, G2, H1, H2, I1, I2, J1 and J2) respectively. Arrows indicate positively labelled osteocytes.

(K) Lineage contribution rate towards PDL or alveolar bone was measured by quantifying percentages of tdTomato+ cells within the PDL at various time points after induction of *Gli1-Cre^{ERT2};Ai14* or *Gli1-Cre^{ERT2};Ai14;Sost$^{-/-}$* mice.

(L and M) Wild type and *Sost$^{-/-}$* mice of 8 month old were harvested for μCT analysis. Dotted lines in (L) and (M) indicate where sections L1, L2, M1 and M2 were acquired. Asterisks indicate alveolar bone. P.I., post-induction.

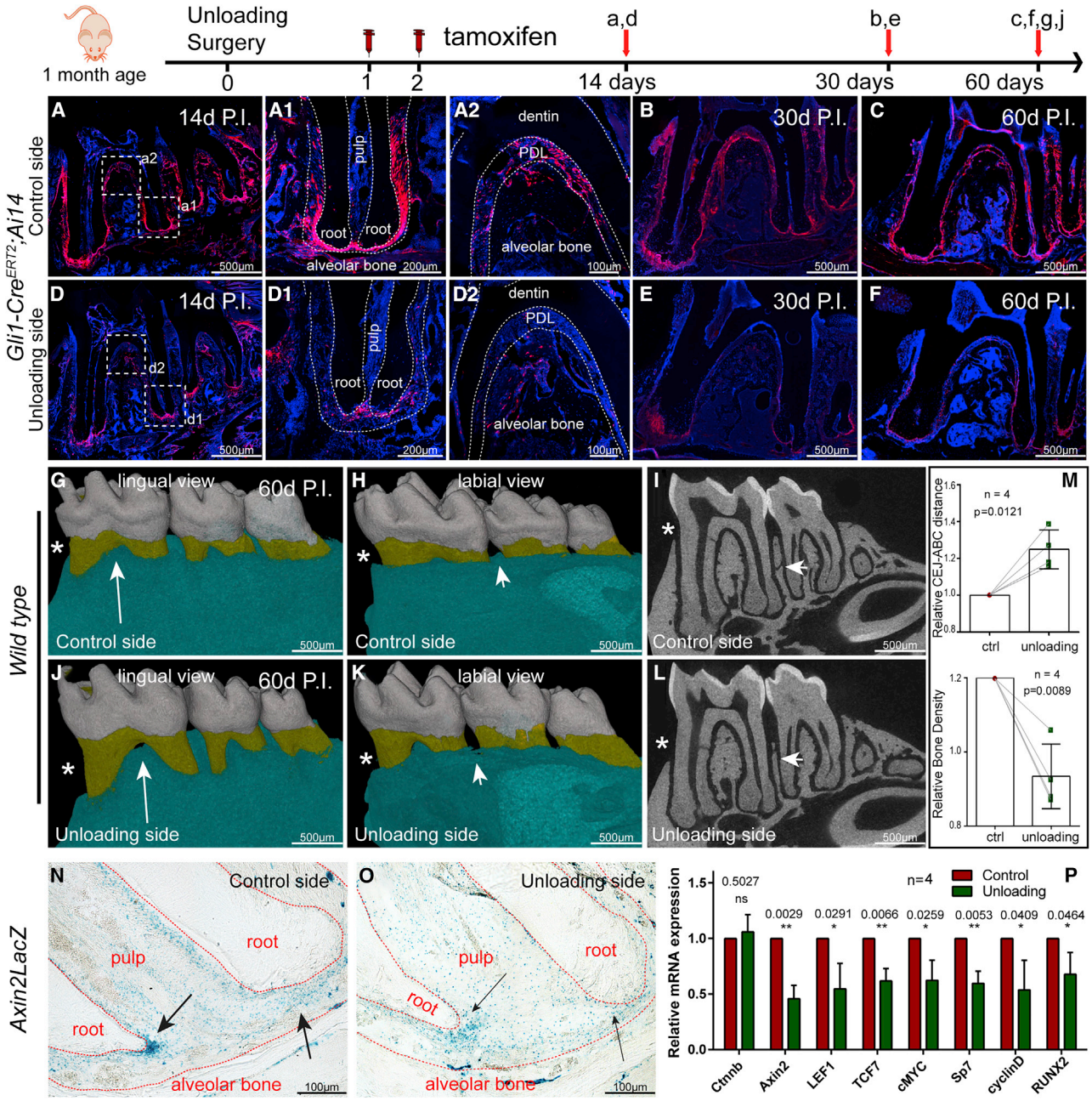

Figure 6. Unloading of Occlusal Force Reduces Both Gli1+ PDLSCs and Canonical Wnt Activity within the Periodontium

Gli1-Cre^{ERT2};Ai14 mice were used for unloading experiments.

(A–C) Molars of the control side were collected on different days after tamoxifen injection. Boxed regions in (A) were enlarged in (A1 and A2) respectively.

(D–F) Molars of the unloading side were collected on different days after tamoxifen injection. Boxed regions in (D) were enlarged in (D1 and D2) respectively.

(G–I) μCT images of control (G–I) and unloading (J–L) side molars acquired 60 days after treatment. Asterisks indicate alveolar bone at the mesial side of the first molar. Arrows indicate alveolar bone in the furcation region. Arrowheads indicate alveolar bone at the interdental bone septum.

(M) Changes in alveolar bone height and bone density were quantified. **p < 0.01, n = 4.

(N and O) Unloading experiments were performed on adult *Axin2-LacZ* mice. Lower molars were collected for LacZ staining one week after unloading. Arrows indicate positive signal.

(P) Periodontium tissues were collected from wild type mice one week after unloading experiments for real-time PCR experiments. P.I., post-induction. **p < 0.01, n = 4. Results are displayed as mean ± SD.

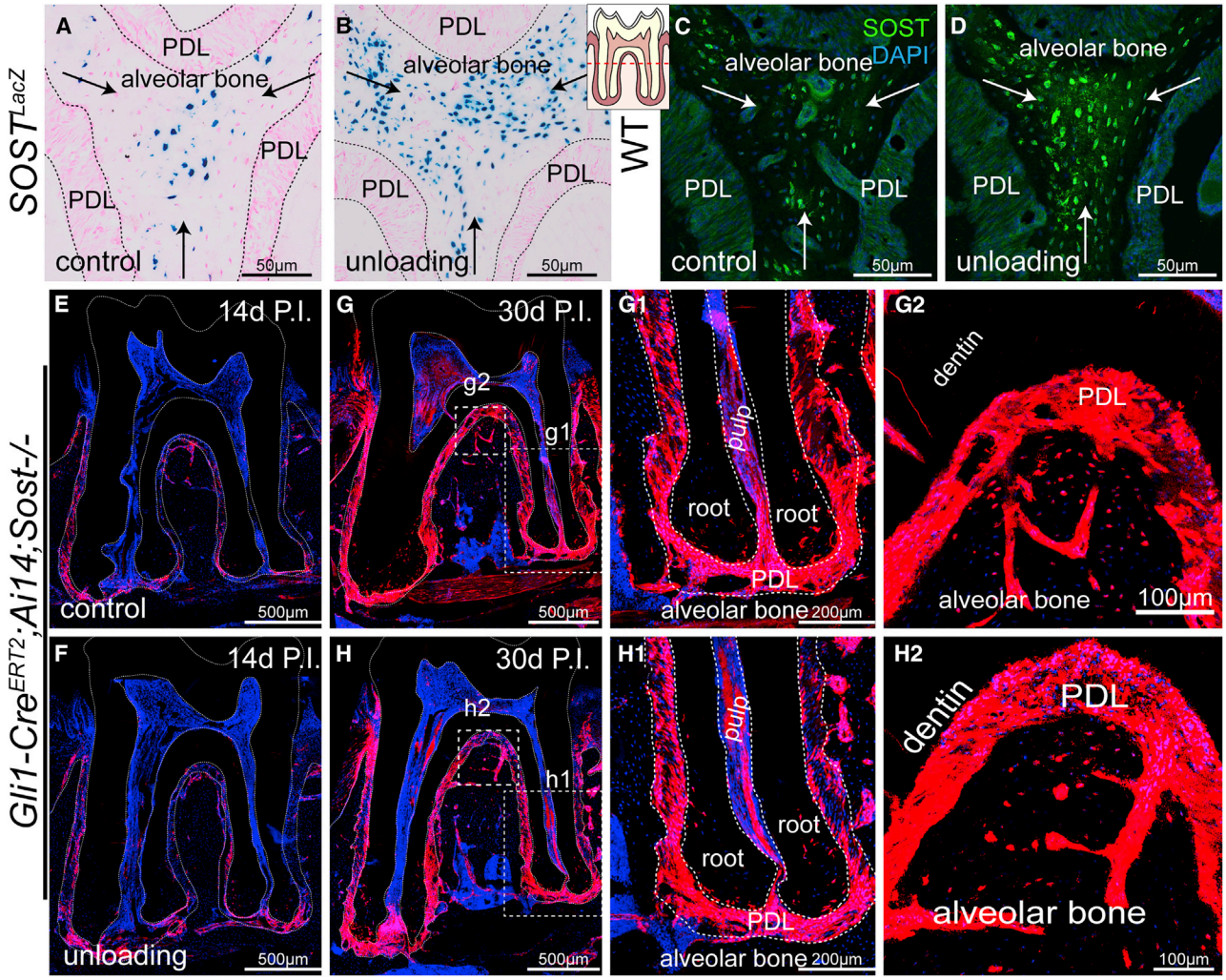

Figure 7. Unloading Increases *Sost* Expression Level and Knockout of *Sost* Eliminates the Alteration of Gli1+ PDLSC Activity by Unloading

Unloading experiments were performed on $Sost^{LacZ}$ or wild type mice.

(A and B) LacZ staining was performed on horizontal sections of the control (A) or unloading side molars (B). Insert indicates position of the sections. Arrows indicate signal.

(C and D) Sclerostin antibody staining on horizontal sections of the control side (C) or unloading side molars (D). Arrows indicate signal. Adult *Gli1-*Cre^{ERT2}*;Ai14;*$Sost^{-/-}$ mice were used for unloading experiments.

(E–H) Molars of the control side were harvested on day 14 (E) or 30 (G) after tamoxifen induction. Boxed regions are enlarged in (G1 and G2) respectively. Molars of the unloading side were harvested on day 14 (F) or 30 (H) after tamoxifen induction. Boxed regions are enlarged in (H1 and H2) respectively. P.I., post-induction.

These results indicated that blockage of *Sclerostin* upregulates Wnt activity within the niche. Contribution of Gli1+ cells toward the PDL and osteocytes were also enhanced.

Physiological Occlusal Force Regulates Gli1+ PDLSCs and Canonical Wnt Activity Level within the Periodontium

To investigate the impact of physiological occlusal force on PDLSCs, the upper molars on one side were extracted from adult *Gli1-*Cre^{ERT2}*;Ai14* mice to unload opposing lower molars. Tamoxifen induction was performed after extraction. On day 14 after induction, fewer tdTomato+ cells were detected in the periodontium of teeth on the unloaded side (Figures 6A–6A2 and 6D–6D2). On days 30 and 60 after induction, the difference between control and unloaded-side teeth was more dramatic (Figures 6B, 6C, 6E, and 6F). On day 60 after induction, the alveolar bone height, indicated by the cementum enamel junction-alveolar bone crest (CEJ-ABC) distance, and the relative bone density were significantly lower than on the control side (Figures 6G–6L). The difference was more dramatic in the furcation and interdental septum regions (white asterisks and arrows in Figures 6G–6L). The results were confirmed with quantitative analysis (Figure 6M).

Unloading experiments were also performed on *Axin2-LacZ* mice. LacZ staining indicated that *Axin2* activity in the apical region of unloaded molars was lower than on the control side (Figures 6N and 6O). Real-time PCR performed with RNA extracted from periodontium tissue indicated that expression levels of *Axin2, Tcf7, Lef1, cMyc, CyclinD*, *Runx2*, and *Sp7* on the

unloaded side were significantly lower than on the control side (Figure 6P).

These results indicated that physiological occlusal force is essential for activation of Gli1+ PDLSCs. Unloading arrested Gli1+ cell activation resulted in PDL tissue loss and reduced Wnt activity.

Knockout of *Sost* Eliminates the Response of Gli1+ PDLSCs to Unloading

Mechanical force is known to inhibit *Sost* expression level in long bone (Robling et al., 2008). To investigate whether occlusal force affects *Sost* expression in the periodontium, unloading experiments were performed on adult *Sost-LacZ* mice. Mandibles were collected one week after unloading and processed for LacZ staining or immunofluorescent staining with sclerostin antibody (Figures 7A–7D). More *Sost*+ osteocytes were visualized within the alveolar bone on the unloaded side (Figures 7B and 7D) than the control side of the mandible (Figures 7A and 7C). Next, unloading experiments were performed on adult *Gli1-Cre^{ERT2};Ai14;Sost$^{-/-}$* mice (Figures 7E–7H). Mandibles were collected on day 14 or 30 after induction. At both time points, similar amounts of tdTomato+ cells were visualized within the PDL of the control and unloaded sides (Figures 7E–7H). This indicates that blockage of *Sost* eliminates the response of Gli1+ cells to mechanical force.

DISCUSSION

PDL, cementum and alveolar bone all originate from cranial neural crest cells during embryonic development (Chai et al., 2000). Our study showed that they also share a common stem cell population during adult homeostasis. A very few numbers of Gli1+ cells (~5%) within the PDL give rise to 95% of PDL cells, 55% of cementoblasts, and 10% of alveolar bone osteocytes within two months. Eight months after induction, these Gli1+ cells continue to contribute to the entire PDL (99%), cementoblast (93%), and alveolar bone osteocyte (85%). Although Gli1+ cells are negative for periodontium lineage differentiation markers, *in vivo* clonal assay shows that individual Gli1+ cells can give rise to PDL cells, cementoblast, and osteocyte and are therefore multipotential. Multipotential capability of Gli1+ cells explains the formation of PDL Sharpey's fibers, which have two ends embedded within the cementum and the alveolar bone respectively. The sandwich-like organization is essential for PDL to hang the teeth within the bone socket. Interestingly, although Gli1+ cells within the apical pulp contribute to dentin and root pulp during root development (Feng et al., 2017), adult Gli1+ PDLSCs make little contribution to odontoblasts despite of some sporadic expression within the pulp. This may be attributed to the fact that dentin tissue within adult molars undergoes little turnover.

We tested other putative stem cell populations marked by αSMA, LepR, NG2, and Pdgfrα (Zhu et al., 2011; Zhou et al., 2014; Miwa and Era, 2018; Pang et al., 2016). None of them significantly contributed to periodontium tissue in our lineage tracing analysis (Roguljic et al., 2013). Axin2, another periodontium progenitor marker, was widely expressed by odontoblasts, cementoblasts, and osteoblasts and therefore is not specific enough (Lohi et al., 2010; Lim et al., 2014).

Gli1+ cells within the PDL are negative for markers of endothelium (GS-IB4), neural or glial cells (β3-tubulin, S100), pericyte (NG2, LepR), or smooth muscle cells (αSMA) and surround the vasculature exclusively. This is similar to Gli1+ stem cells within the incisor mesenchyme (Zhao et al., 2014). We believe the Gli1+ PDLSCs are located within the tunica adventitia of large blood vessels accompanying the NVB and possess fibroblast-like cellular properties. Deep imaging revealed that nerves and blood vessels from the PDL and dental pulp converged at in the apical region. This explains why Gli1+ cells are more enriched near the apical region. SHH was known to be the hedgehog ligand in rodent teeth (Seidel et al., 2010). During embryonic and early postnatal development, SHH is mainly secreted by dental epithelium, which gradually disappears in molars after P21 (Li et al., 2015). Nerves as another source of SHH ligand maintain its expression in adulthood. SHH ligand secreted from the trigeminal ganglion neurons was transported along the IAN to the incisor to regulate stem cell differentiation (Zhao et al., 2014). Here, we confirmed the *Shh* expression within the trigeminal ganglion, IAN, and nerve axons within the apical PDL. SHH may have similar regulating functions to Gli1+ PDLSCs as in the incisor. Indeed, denervation has been shown to cause altered occlusal height, dental-alveolar ankylosis, and alveolar bone loss, and these phenotypes were unrelated to vasculature damage (Kim et al., 2009; Fujiyama et al., 2004; Zhang et al., 2003), suggesting roles of nerves on regulating periodontium tissue.

Canonical Wnt signaling plays critical regulating roles in various stem cell populations including periodontium Axin2+ PDL cells (An et al., 2018; Lim et al., 2014). Our loss-of-function and gain-of-function experiments indicated that Wnt signal is essential for Gli1+ PDLSCs activation. In the absence of Wnt signal, Gli1+ PDLSCs failed to activate which finally led to severe periodontium tissue loss. Wnt activity was only detected within a small portion of Gli1+ cells. This may be attributed to the fact that Gli1+ PDLSCs are overall quiescent and only a few cells need to be activated under physiological conditions. Injury can activate these quiescent Gli1+ stem cells into proliferation.

Wnt signaling was rarely regulated in an on or off fashion under physiological conditions. More often, the signal intensity was modulated by other signaling pathways or Wnt inhibitors including DKK1, DKK3, WIF1, and sclerostin (Kosinski et al., 2010; Planas-Paz et al., 2016; Lim et al., 2013; Semënov et al., 2005). Sclerostin is a canonical Wnt inhibitor, which binds to LRP4 and interrupt the binding of low-density lipoprotein receptor-related protein 5 or 6 with Wnt ligands (Semënov et al., 2005; Xiong et al., 2015). It remains unknown if sclerostin regulates stem cells activities *in vivo*. Our study revealed a role played by sclerostin within the stem cell niche. We showed that sclerostin ligand negatively regulates both Wnt and Gli1+ PDLSCs activities. Knockout of *Sost* upregulated the Wnt activity level and accelerated the Gli1+ PDLSCs lineage contribution rate toward PDL and osteocyte. Sclerostin was known to inhibit osteoblast differentiation (Koide and Kobayashi, 2019; Robling et al., 2008; Tu et al., 2012). The increased bone formation in the *Sost$^{-/-}$* mouse mandible can be attributed to its combinatorial actions upon both osteoblast and PDLSCs. *Sost* was expressed by both alveolar bone and cementoblast on the root surface. We speculate regulation roles of cementoblast are relatively minor due to the low cementoblast number.

Mechanical force regulates many stem cell populations. Unloaded molar is an excellent model on studying mechanical regulation because non-treated contra-lateral molars provides an internal control (Morey et al., 1979; Hinton et al., 2018). With this model, we showed that mechanical force is essential for the activation of Gli1+ PDLSCs. Removal of occlusal force downregulated Wnt activity and arrested Gli1+ cells activation. We further demonstrated that the mechano-response was indirectly mediated by sclerostin ligand secreted from the osteocytes because blockage of sclerostin completely eliminated the mechano-response behavior of Gli1+ cells. Our results are consistent with previous studies, which showed association between Sclerostin, osteogenesis, and mechanical loading within long bones (Robling et al., 2008; Koide and Kobayashi, 2019; Tu et al., 2012) or within alveolar bone (Shu et al., 2017; Odagaki et al., 2018; Ueda et al., 2016). Tissue loss phenotypes after unloading were much less severe than in the *β-catenin* inducible knockout mutant mice, suggesting other signaling pathways may also be affected by unloading and counteracted Wnt signaling change.

In summary, our study identified Gli1+ cells as multipotential stem cells for the periodontium tissue. Canonical Wnt signaling is critical for their activation. Sclerostin from the osteocyte is a negative feedback regulator for Gli1+ PDLSCs activity. Furthermore, occlusal force indirectly regulates Gli1+ stem cells by fine-tuning the feedback loop.

STAR★METHODS

Detailed methods are provided in the online version of this paper and include the following:

- KEY RESOURCES TABLE
- RESOURCE AVAILABILITY
  - Lead Contact
  - Materials Availability
  - Data and Code Availability
- EXPERIMENTAL MODEL AND SUBJECT DETAILS
  - Mice
  - Animal Care and Use
- METHODS DETAILS
  - Periodontium Cell Culture
  - Tamoxifen Administration
  - Mice Perfusion and Sample Harvest
  - Mice PDL injury assay
  - Immunofluorescent and GS-IB4 Staining
  - X-gal Staining
  - Long Duration EdU Incorporation Assay
  - PEGASOS Tissue Clearing and 3D Image Acquisition
  - Occlusal Force Unloading Experiment
  - Real Time-PCR and Analysis
  - Periodontium Cells Differentiation Assay
  - MicroCT Scanning and Analysis
- QUANTIFICATION AND STATISTICAL ANALYSIS

SUPPLEMENTAL INFORMATION

Supplemental Information can be found online at https://doi.org/10.1016/j.devcel.2020.06.006.

ACKNOWLEDGMENTS

We thank Dr. Kate Phelps for technical support with microscopy. We thank Dr. Sean Morrison in the UTSW for providing *LepR+;Ai14* mice. Sost-lacZ mice were from Regeneron Pharmaceuticals in Tarrytown, New York with a Material Transfer Agreement to Jian Feng. We thank Drs. Zhihe Zhao, Jun Wang, and Quan Yuan in the Sichuan University for technical support. This work was supported by startup funding from Texas A&M University, NIH/NIDCR grants K08DE025090, R01 DE028291, and R21 DE027928 to H. Z. and R01 DE025659 to J.F.

AUTHOR CONTRIBUTIONS

H.Z. designed and supervised the study. Y.M. performed most of the experiments. Y.W. contributed to the manuscript revision. D.J., Y.Y., W.L., W.S., J.Q.F., and Y.C. contributed to data acquisition. B.S. and W.-P.G. contributed to data analysis. The manuscript was written by H.Z. and Y.M. All authors gave final approval and agreed to be accountable for all aspects of the work.

DECLARATION OF INTERESTS

The authors declare no competing interests.

Received: May 24, 2019
Revised: February 4, 2020
Accepted: June 2, 2020
Published: July 10, 2020

REFERENCES

Acar, M., Kocherlakota, K.S., Murphy, M.M., Peyer, J.G., Oguro, H., Inra, C.N., Jaiyeola, C., Zhao, Z., Luby-Phelps, K., and Morrison, S.J. (2015). Deep imaging of bone marrow shows non-dividing stem cells are mainly perisinusoidal. Nature *526*, 126–130.

An, Z., Akily, B., Sabalic, M., Zong, G., Chai, Y., and Sharpe, P.T. (2018). Regulation of mesenchymal stem to transit-amplifying cell transition in the continuously growing mouse incisor. Cell Rep *23*, 3102–3111.

Arnold, T.D., Ferrero, G.M., Qiu, H., Phan, I.T., Akhurst, R.J., Huang, E.J., and Reichardt, L.F. (2012). Defective retinal vascular endothelial cell development as a consequence of impaired integrin integrin αVβ8-mediated activation of transforming growth factor-β. J. Neurosci. *32*, 1197–1206.

Balic, A., and Thesleff, I. (2015). Tissue interactions regulating tooth development and renewal. Curr. Top. Dev. Biol. *115*, 157–186.

Chai, Y., Jiang, X., Ito, Y., Bringas, P., Han, J., Rowitch, D.H., Soriano, P., McMahon, A.P., and Sucov, H.M. (2000). Fate of the mammalian cranial neural crest during tooth and mandibular morphogenesis. Development *127*, 1671–1679.

Chang, L., Azzolin, L., Di Biagio, D., Zanconato, F., Battilana, G., Lucon Xiccato, R., Aragona, M., Giulitti, S., Panciera, T., Gandin, A., et al. (2018). The SWI/SNF complex is a mechanoregulated inhibitor of YAP and TAZ. Nature *563*, 265–269.

Collette, N.M., Genetos, D.C., Economides, A.N., Xie, L., Shahnazari, M., Yao, W., Lane, N.E., Harland, R.M., and Loots, G.G. (2012). Targeted deletion of Sost distal enhancer increases bone formation and bone mass. Proc. Natl. Acad. Sci. USA *109*, 14092–14097.

Cosgrove, B.D., Mui, K.L., Driscoll, T.P., Caliari, S.R., Mehta, K.D., Assoian, R.K., Burdick, J.A., and Mauck, R.L. (2016). N-cadherin adhesive interactions modulate matrix mechanosensing and fate commitment of mesenchymal stem cells. Nat. Mater. *15*, 1297–1306.

Degirmenci, B., Valenta, T., Dimitrieva, S., Hausmann, G., and Basler, K. (2018). GLI1-expressing mesenchymal cells form the essential Wnt-secreting niche for colon stem cells. Nature *558*, 449–453.

Delgado-Calle, J., Sato, A.Y., and Bellido, T. (2017). Role and mechanism of action of sclerostin in bone. Bone *96*, 29–37.

Epah, J., Pálfi, K., Dienst, F.L., Malacarne, P.F., Bremer, R., Salamon, M., Kumar, S., Jo, H., Schürmann, C., and Brandes, R.P. (2018). 3D imaging

and quantitative analysis of vascular networks: a comparison of ultramicroscopy and micro-computed tomography. Theranostics *8*, 2117–2133.

Farin, H.F., Jordens, I., Mosa, M.H., Basak, O., Korving, J., Tauriello, D.V., De Punder, K., Angers, S., Peters, P.J., Maurice, M.M., and Clevers, H. (2016). Visualization of a short-range Wnt gradient in the intestinal stem-cell niche. Nature *530*, 340–343.

Feng, J., Jing, J., Li, J., Zhao, H., Punj, V., Zhang, T., Xu, J., and Chai, Y. (2017). BMP signaling orchestrates a transcriptional network to control the fate of mesenchymal stem cells in mice. Development *144*, 2560–2569.

Fujiyama, K., Yamashiro, T., Fukunaga, T., Balam, T.A., Zheng, L., and Takano-Yamamoto, T. (2004). Denervation resulting in dento-alveolar ankylosis associated with decreased Malassez epithelium. J. Dent. Res. *83*, 625–629.

Guo, L., Cai, T., Chen, K., Wang, R., Wang, J., Cui, C., Yuan, J., Zhang, K., Liu, Z., Deng, Y., et al. (2018). Kindlin-2 regulates mesenchymal stem cell differentiation through control of YAP1/TAZ. J. Cell Biol. *217*, 1431–1451.

Harada, N., Tamai, Y., Ishikawa, T., Sauer, B., Takaku, K., Oshima, M., and Taketo, M.M. (1999). Intestinal polyposis in mice with a dominant stable mutation of the beta-catenin gene. EMBO J *18*, 5931–5942.

Hinton, P.V., Rackard, S.M., and Kennedy, O.D. (2018). In vivo osteocyte mechanotransduction: recent developments and future directions. Curr. Osteoporos. Rep. *16*, 746–753.

Hooper, A.T., Butler, J.M., Nolan, D.J., Kranz, A., Iida, K., Kobayashi, M., Kopp, H.G., Shido, K., Petit, I., Yanger, K., et al. (2009). Engraftment and reconstitution of hematopoiesis is dependent on VEGFR2-mediated regeneration of sinusoidal endothelial cells. Cell Stem Cell *4*, 263–274.

Horiuchi, K., Amizuka, N., Takeshita, S., Takamatsu, H., Katsuura, M., Ozawa, H., Toyama, Y., Bonewald, L.F., and Kudo, A. (1999). Identification and characterization of a novel protein, periostin, with restricted expression to periosteum and periodontal ligament and increased expression by transforming growth factor beta. J. Bone Miner. Res. *14*, 1239–1249.

Ivanovski, S., Gronthos, S., Shi, S., and Bartold, P.M. (2006). Stem cells in the periodontal ligament. Oral Dis *12*, 358–363.

Järvinen, E., Shimomura-Kuroki, J., Balic, A., Jussila, M., and Thesleff, I. (2018). Mesenchymal Wnt/beta-catenin signaling limits tooth number. Development *145*.

Jeong, H.W., Hernández-Rodríguez, B., Kim, J., Kim, K.P., Enriquez-Gasca, R., Yoon, J., Adams, S., Schöler, H.R., Vaquerizas, J.M., and Adams, R.H. (2017). Transcriptional regulation of endothelial cell behavior during sprouting angiogenesis. Nat. Commun. *8*, 726.

Jing, D., Zhang, S., Luo, W., Gao, X., Men, Y., Ma, C., Liu, X., Yi, Y., Bugde, A., Zhou, B.O., et al. (2018). Tissue clearing of both hard and soft tissue organs with the PEGASOS method. Cell Res *28*, 803–818.

Kim, Y., Hamada, N., Takahashi, Y., Sasaguri, K., Tsukinoki, K., Onozuka, M., and Sato, S. (2009). Cervical sympathectomy causes alveolar bone loss in an experimental rat model. J. Periodont. Res. *44*, 695–703.

Koide, M., and Kobayashi, Y. (2019). Regulatory mechanisms of sclerostin expression during bone remodeling. J. Bone Miner. Metab. *37*, 9–17.

Kosinski, C., Stange, D.E., Xu, C., Chan, A.S., Ho, C., Yuen, S.T., Mifflin, R.C., Powell, D.W., Clevers, H., Leung, S.Y., and Chen, X. (2010). Indian hedgehog regulates intestinal stem cell fate through epithelial-mesenchymal interactions during development. Gastroenterology *139*, 893–903.

Kurpinski, K., Chu, J., Hashi, C., and Li, S. (2006). Anisotropic mechanosensing by mesenchymal stem cells. Proc. Natl. Acad. Sci. USA *103*, 16095–16100.

Lan, Y., Jia, S., and Jiang, R. (2014). Molecular patterning of the mammalian dentition. Semin. Cell Dev. Biol. *25–26*, 61–70.

Lee, J.H., Tammela, T., Hofree, M., Choi, J., Marjanovic, N.D., Han, S., Canner, D., Wu, K., Paschini, M., Bhang, D.H., et al. (2017). Anatomically and functionally distinct lung mesenchymal populations marked by Lgr5 and Lgr6. Cell *170*, 1149–1163.e12.

Li, J., Feng, J., Liu, Y., Ho, T.V., Grimes, W., Ho, H.A., Park, S., Wang, S., and Chai, Y. (2015). BMP-SHH signaling network controls epithelial stem cell fate via regulation of its niche in the developing tooth. Dev. Cell *33*, 125–135.

Lim, W.H., Liu, B., Cheng, D., Hunter, D.J., Zhong, Z., Ramos, D.M., Williams, B.O., Sharpe, P.T., Bardet, C., Mah, S.J., and Helms, J.A. (2014). Wnt signaling regulates pulp volume and dentin thickness. J. Bone Miner. Res. *29*, 892–901.

Lim, X., Tan, S.H., Koh, W.L., Chau, R.M., Yan, K.S., Kuo, C.J., Van Amerongen, R., Klein, A.M., and Nusse, R. (2013). Interfollicular epidermal stem cells self-renew via autocrine Wnt signaling. Science *342*, 1226–1230.

Lin, Z., Fateh, A., Salem, D.M., and Intini, G. (2014). Periosteum: biology and applications in craniofacial bone regeneration. J. Dent. Res. *93*, 109–116.

Liu, F., Chu, E.Y., Watt, B., Zhang, Y., Gallant, N.M., Andl, T., Yang, S.H., Lu, M.M., Piccolo, S., Schmidt-Ullrich, R., et al. (2008). Wnt/beta-catenin signaling directs multiple stages of tooth morphogenesis. Dev. Biol. *313*, 210–224.

Lohi, M., Tucker, A.S., and Sharpe, P.T. (2010). Expression of Axin2 indicates a role for canonical Wnt signaling in development of the crown and root during pre- and postnatal tooth development. Dev. Dyn. *239*, 160–167.

Maruyama, T., Jeong, J., Sheu, T.J., and Hsu, W. (2016). Stem cells of the suture mesenchyme in craniofacial bone development, repair and regeneration. Nat. Commun. *7*, 10526.

Meng, Z., Qiu, Y., Lin, K.C., Kumar, A., Placone, J.K., Fang, C., Wang, K.C., Lu, S., Pan, M., Hong, A.W., et al. (2018). RAP2 mediates mechanoresponses of the Hippo pathway. Nature *560*, 655–660.

Miwa, H., and Era, T. (2018). Tracing the destiny of mesenchymal stem cells from embryo to adult bone marrow and white adipose tissue via Pdgfralpha expression. Development *145*.

Morey, E.R., Sabelman, E.E., Turner, R.T., and Baylink, D.J. (1979). A new rat model simulating some aspects of space flight. Physiologist *22*, S23–S24.

Odagaki, N., Ishihara, Y., Wang, Z., Ei Hsu Hlaing, E., Nakamura, M., Hoshijima, M., Hayano, S., Kawanabe, N., and Kamioka, H. (2018). Role of osteocyte-PDL crosstalk in tooth movement via SOST/sclerostin. J. Dent. Res. *97*, 1374–1382.

Ohle, S.J., Anandaiah, A., Fabian, A.J., Fine, A., and Kotton, D.N. (2012). Maintenance and repair of the lung endothelium does not involve contributions from marrow-derived endothelial precursor cells. Am J Respir Cell Mol Biol *47*, 11–19.

Ono, W., Sakagami, N., Nishimori, S., Ono, N., and Kronenberg, H.M. (2016). Parathyroid hormone receptor signalling in osterix-expressing mesenchymal progenitors is essential for tooth root formation. Nat. Commun. *7*, 11277.

Pang, Y.W., Feng, J., Daltoe, F., Fatscher, R., Gentleman, E., Gentleman, M.M., and Sharpe, P.T. (2016). Perivascular stem cells at the tip of mouse incisors regulate tissue regeneration. J. Bone Miner. Res. *31*, 514–523.

Planas-Paz, L., Orsini, V., Boulter, L., Calabrese, D., Pikiolek, M., Nigsch, F., Xie, Y., Roma, G., Donovan, A., Marti, P., et al. (2016). The RSPO-LGR4/5-ZNRF3/RNF43 module controls liver zonation and size. Nat. Cell Biol. *18*, 467–479.

Robling, A.G., Niziolek, P.J., Baldridge, L.A., Condon, K.W., Allen, M.R., Alam, I., Mantila, S.M., Gluhak-Heinrich, J., Bellido, T.M., Harris, S.E., and Turner, C.H. (2008). Mechanical stimulation of bone in vivo reduces osteocyte expression of Sost/sclerostin. J. Biol. Chem. *283*, 5866–5875.

Roguljic, H., Matthews, B.G., Yang, W., Cvija, H., Mina, M., and Kalajzic, I. (2013). In vivo identification of periodontal progenitor cells. J. Dent. Res. *92*, 709–715.

Schneider, R.K., Mullally, A., Dugourd, A., Peisker, F., Hoogenboezem, R., Van Strien, P.M.H., Bindels, E.M., Heckl, D., Büsche, G., Fleck, D., et al. (2017). Gli1+ mesenchymal stromal cells are a key driver of bone marrow fibrosis and an important cellular therapeutic target. Cell Stem Cell *20*, 785–800.e8.

Seidel, K., Ahn, C.P., Lyons, D., Nee, A., Ting, K., Brownell, I., Cao, T., Carano, R.A., Curran, T., Schober, M., et al. (2010). Hedgehog signaling regulates the generation of ameloblast progenitors in the continuously growing mouse incisor. Development *137*, 3753–3761.

Semënov, M., Tamai, K., and He, X. (2005). SOST is a ligand for LRP5/LRP6 and a Wnt signaling inhibitor. J. Biol. Chem. *280*, 26770–26775.

Seo, B.M., Miura, M., Gronthos, S., Bartold, P.M., Batouli, S., Brahim, J., Young, M., Robey, P.G., Wang, C.Y., and Shi, S. (2004). Investigation of multipotent postnatal stem cells from human periodontal ligament. Lancet *364*, 149–155.

Shi, Y., He, G., Lee, W.C., Mckenzie, J.A., Silva, M.J., and Long, F. (2017). Gli1 identifies osteogenic progenitors for bone formation and fracture repair. Nat. Commun. *8*, 2043.

Shu, R., Bai, D., Sheu, T., He, Y., Yang, X., Xue, C., He, Y., Zhao, M., and Han, X. (2017). Sclerostin promotes bone remodeling in the process of tooth movement. PLoS One *12*, e0167312.

Sörensen, I., Adams, R.H., and Gossler, A. (2009). DLL1-mediated Notch activation regulates endothelial identity in mouse fetal arteries. Blood *113*, 5680–5688.

Takahashi, A., Nagata, M., Gupta, A., Matsushita, Y., Yamaguchi, T., Mizuhashi, K., Maki, K., Ruellas, A.C., Cevidanes, L.S., Kronenberg, H.M., et al. (2019). Autocrine regulation of mesenchymal progenitor cell fates orchestrates tooth eruption. Proc. Natl. Acad. Sci. USA *116*, 575–580.

Ten Cate, A.R. (1997). The development of the periodontium–a largely ectomesenchymally derived unit. Periodontol. 2000 *13*, 9–19.

Tran, Hle B., Doan, V.N., Le, H.T., and Ngo, L.T. (2014). Various methods for isolation of multipotent human periodontal ligament cells for regenerative medicine. In Vitro Cell. Dev. Biol. Anim. *50*, 597–602.

Tu, X., Rhee, Y., Condon, K.W., Bivi, N., Allen, M.R., Dwyer, D., Stolina, M., Turner, C.H., Robling, A.G., Plotkin, L.I., and Bellido, T. (2012). Sost downregulation and local Wnt signaling are required for the osteogenic response to mechanical loading. Bone *50*, 209–217.

Ueda, M., Kuroishi, K.N., Gunjigake, K.K., Ikeda, E., and Kawamoto, T. (2016). Expression of Sost/sclerostin in compressed periodontal ligament cells. J. Dent. Sci. *11*, 272–278.

Wang, B., Zhao, L., Fish, M., Logan, C.Y., and Nusse, R. (2015). Self-renewing diploid Axin2(+) cells fuel homeostatic renewal of the liver. Nature *524*, 180–185.

Wendling, O., Bornert, J.M., Chambon, P., and Metzger, D. (2009). Efficient temporally-controlled targeted mutagenesis in smooth muscle cells of the adult mouse. Genesis *47*, 14–18.

Xiong, L., Jung, J.U., Wu, H., Xia, W.F., Pan, J.X., Shen, C., Mei, L., and Xiong, W.C. (2015). Lrp4 in osteoblasts suppresses bone formation and promotes osteoclastogenesis and bone resorption. Proc. Natl. Acad. Sci. USA *112*, 3487–3492.

Xu, C., Gao, X., Wei, Q., Nakahara, F., Zimmerman, S.E., Mar, J., and Frenette, P.S. (2018). Stem cell factor is selectively secreted by arterial endothelial cells in bone marrow. Nat. Commun. *9*, 2449.

Xu, Q., Yuan, X., Zhang, X., Chen, J., Shi, Y., Brunski, J.B., and Helms, J.A. (2019). Mechanoadaptive responses in the periodontium are coordinated by Wnt. J. Dent. Res. *98*, 689–697.

Yin, X., Li, J., Salmon, B., Huang, L., Lim, W.H., Liu, B., Hunter, D.J., Ransom, R.C., Singh, G., Gillette, M., et al. (2015). Wnt signaling and its contribution to craniofacial tissue homeostasis. J. Dent. Res. *94*, 1487–1494.

Zhang, W., Kobayashi, M., Moritani, M., Masuda, Y., Dong, J., Yagi, T., Maeda, T., and Morimoto, T. (2003). An involvement of trigeminal mesencephalic neurons in regulation of occlusal vertical dimension in the guinea pig. J. Dent. Res. *82*, 565–569.

Zhang, X., Yuan, X., Xu, Q., Arioka, M., Van Brunt, L.A., Shi, Y., Brunski, J., and Helms, J.A. (2019). Molecular basis for periodontal ligament adaptation to in vivo loading. J. Dent. Res. *98*, 331–338.

Zhao, H., Feng, J., Ho, T.V., Grimes, W., Urata, M., and Chai, Y. (2015). The suture provides a niche for mesenchymal stem cells of craniofacial bones. Nat. Cell Biol. *17*, 386–396.

Zhao, H., Feng, J., Seidel, K., Shi, S., Klein, O., Sharpe, P., and Chai, Y. (2014). Secretion of shh by a neurovascular bundle niche supports mesenchymal stem cell homeostasis in the adult mouse incisor. Cell Stem Cell *14*, 160–173.

Zhou, B.O., Yue, R., Murphy, M.M., Peyer, J.G., and Morrison, S.J. (2014). Leptin-receptor-expressing mesenchymal stromal cells represent the main source of bone formed by adult bone marrow. Cell Stem Cell *15*, 154–168.

Zhu, X., Hill, R.A., Dietrich, D., Komitova, M., Suzuki, R., and Nishiyama, A. (2011). Age-dependent fate and lineage restriction of single NG2 cells. Development *138*, 745–753.

STAR★METHODS

KEY RESOURCES TABLE

REAGENT or RESOURCE	SOURCE	IDENTIFIER
Antibodies		
Rat monoclonal anti-CD44	BD Biosciences	Cat# 561859, RRID:AB_10894581
Rat monoclonal anti-CD73	BD Biosciences	Cat# 561545, RRID:AB_10714516
Rat monoclonal anti-CD146	BD Biosciences	Cat# 562229, RRID:AB_11153320
Rabbit polyclonal anti-Periostin	Abcam	Cat# ab14041, RRID:AB_372585
Rabbit polyclonal anti-Collagen I	Abcam	Cat# ab21286, RRID:AB_446161
Rabbit polyclonal anti-Sp7/Osterix	Abcam	Cat# ab22552, RRID:AB_2194492
Mouse monoclonal anti-Neuron-specific beta-III Tubulin	R&D system	Cat# MAB1195, RRID:AB_357520
Mouse monoclonal anti-Actin α-Smooth Muscle, FITC Conjugated	Sigma-Aldrich	Cat# F3777, RRID:AB_476977
Goat polyclonal anti-Mouse Leptin R	R&D system	Cat# AF497, RRID:AB_2281270
Chicken polyclonal anti-beta Galactosidase	Immunology Consultants Laboratory	Cat# CGAL-45A-Z, RRID:AB_2756355
Goat polyclonal anti-Mouse SOST/ Sclerostin	R&D system	Cat# AF1589, RRID:AB_2195345
Rabbit polyclonal anti-Perilipin A	Abcam	Cat# ab3526, RRID:AB_2167274
Rabbit polyclonal anti-CD31	Abcam	Cat# ab28364, RRID:AB_726362
Rat monoclonal anti-CD34	BD Biosciences	Cat# 560238, RRID:AB_1645242
Mouse monoclonal anti-Nestin	Millipore	Cat# MAB353, RRID:AB_94911
Anti-NG2 Chondroitin Sulfate Proteoglycan Antibody	Millipore	Cat# AB5320, RRID:AB_91789
PDGFRa	eBioscience	Cat# 14-1401-82, RRID:AB_467491
Anti-Sonic Hedgehog antibody	Abcam	Cat# ab50515, RRID:AB_882647
Mouse IgG1 Isotype Control	R&D system	Cat# MAB002, RRID:AB_357344
Mouse IgG2A Isotype Control	R&D system	Cat# MAB003, RRID:AB_357345
FITC Rat IgG2b, κ Isotype Control	BD Biosciences	Cat# 553988, RRID:AB_479619
Rat IgG2a, κ Isotype Control	BD Biosciences	Cat# 562302, RRID:AB_11154396
Rabbit IgG, polyclonal - Isotype Control	Abcam	Cat# ab37415, RRID:AB_2631996
Normal Goat IgG Control	R&D system	Cat# AB-108-C, RRID:AB_354267
Normal Chicken IgY Control	R&D system	Cat# AB-101-C, RRID:AB_354263
Goat polyclonal anti-Mouse IgG(H+L) Alexa Fluor 488	Invitrogen	Cat# A-11029, RRID:AB_138404
Goat polyclonal anti-Rat IgG(H+L) Alexa Fluor 488	Invitrogen	Cat# A-11006, RRID:AB_141373
Goat polyclonal anti-Rabbit IgG(H+L) Alexa Fluor 488	Invitrogen	Cat# A-11008, RRID:AB_143165
Goat polyclonal anti-Chicken IgY(H+L) Alexa Fluor 488	Abcam	Cat# ab150169, RRID:AB_2636803
Chemicals, Peptides, and Recombinant Proteins		
DMEM low glucose	Gibco	Cat# 11885084
Fetal Bovine Serum (FBS)	Gibco	Cat# 16140071
L-Glutamine (200 mM)	Gibco	Cat# 25030081
Penicillin-Streptomycin (10,000 U/mL)	Gibco	Cat# 15140122
TrypLE™ Express Enzyme (1X), phenol red	Gibco	Cat# 12605010
Tamoxifen	Sigma-Aldrich	Cat# T5648
Corn oil	Sigma-Aldrich	Cat# C8267

(*Continued on next page*)

Continued

REAGENT or RESOURCE	SOURCE	IDENTIFIER
Ethylenediaminetetraacetic acid disodium salt dihydrate (EDTA)	Sigma-Aldrich	Cat# E5134
Paraformaldehyde (PFA)	Sigma-Aldrich	Cat# P6148
OCT	VWR	Cat# 411243
Isolectin B4 (GS-IB4) Alex488 Conjugated	Invitrogen	Cat# I21411, RRID:AB_2314662
Glutaraldehyde	Sigma-Aldrich	Cat# G6257
Sodium deoxycholate	Sigma-Aldrich	Cat# D6750
IGEPAL® CA-630	Sigma-Aldrich	Cat# I8896
Potassium ferrocyanide(II)	Sigma-Aldrich	Cat# P3289
Potassium ferricyanide(III)	Sigma-Aldrich	Cat# 702587
5-Bromo-4-chloro-3-indolyl β-D-galactopyranoside (X-gal)	Sigma-Aldrich	Cat# B6024
2'-Deoxy-5-ethynyluridine (EdU)	Carbosynth	Cat# NE08701
Nuclear fast red	Sigma-Aldrich	Cat# N8002
Aluminum sulfate	Sigma-Aldrich	Cat# 202614
Eosin Y disodium salt	Sigma-Aldrich	Cat# E6003
Quardol	Sigma-Aldrich	Cat# 122262
tert-Butanol	Sigma-Aldrich	Cat# 360538
PEGMMA500	Sigma-Aldrich	Cat# 409529
Benzyl benzoate	Sigma-Aldrich	Cat# 409529
StemPro™ Osteogenesis Differentiation Kit	Gibco	Cat# A1007201
StemPro™ Chondrogenesis Differentiation Kit	Gibco	Cat# A1007101
StemPro™ Adipogenesis Differentiation Kit	Gibco	Cat# A1007001
Alizarin Red	Sigma-Aldrich	Cat# A5533
Oil Red O	Sigma-Aldrich	Cat# O0625
Alcian Blue	Sigma-Aldrich	Cat# A3157
Sodium Nitrite	Sigma-Aldrich	Cat# 237213
Naphthol AS-BI Phosphate	Sigma-Aldrich	Cat# N2125
Pararosaniline hydrochloride	Sigma-Aldrich	Cat# P3750
Critical Commercial Assays		
Click-iT™ EdU Alexa Fluor™ 488 Imaging Kit	Invitrogen	Cat# C10337
RNeasy Mini Kit	Qiagen	Cat# 79656
5xAll-in-one 1st Strand cDNA Synthesis Mix	Bioland	Cat# FS01
2xqPCR Master Mix	Bioland	Cat# QP01
Experimental Models: Organisms/Strains		
Mouse: C57/B6J	The Jackson Laboratory	Stock No: 000664
Mouse: Gli1$^{tm3(cre/ERT2)Alj}$/J	The Jackson Laboratory	Stock No: 007913
Mouse: B6.Cg-Gt(ROSA)26Sor$^{tm14(CAG-tdTomato)Hze}$/J	The Jackson Laboratory	Stock No: 007914
Mouse: B6.129-Ctnnb1^{tm2Kem}/KnwJ	The Jackson Laboratory	Stock No: 004152
Mouse: B6.Cg-Tg(Syn1-cre)671Jxm/J	The Jackson Laboratory	Stock No: 003966
Mouse: B6N.129P2-Axin2^{tm1Wbm}/J	The Jackson Laboratory	Stock No: 009120
Mouse: B6.129(Cg)-Lepr$^{tm2(cre)Rck}$/J	The Jackson Laboratory	Stock No: 008320
Mouse: B6.Cg-Tg(Cspg4-cre/Esr1*) BAkik/J	The Jackson Laboratory	Stock No: 008538
Mouse: B6N.Cg-Tg(Pdgfra-cre/ER) 467Dbe/J	The Jackson Laboratory	Stock No:018280
Mouse: αSMA-CreERT2	(Wendling et al., 2009)	N/A

(*Continued on next page*)

Continued

REAGENT or RESOURCE	SOURCE	IDENTIFIER
Mouse: Cdh5-CreERT2	(Sörensen et al., 2009)	N/A
Mouse: Ctnnb1$^{flx(ex3)}$	(Harada et al., 1999)	N/A
Mouse: SOST-Lacz	(Collette et al., 2012)	N/A
Oligonucleotides		
Genotyping primers (see Table S1 for primers sequence information)	This paper	N/A
RT-PCR primers (see Table S1 for primers sequence information)	This paper	N/A
Software and Algorithms		
Imaris 9.0	Bitplane	https://imaris.oxinst.com/
ImageJ 1.52k	NIH	https://imagej.nih.gov/ij/
GraphPad Prism 8	GraphPad Spftware Inc	https://www.graphpad.com/scientific-software/prism/

RESOURCE AVAILABILITY

Lead Contact

Further information and requests for resources should be directed to and will be fulfilled by the Lead Contact, Hu Zhao (huzhao@tamu.edu, huzhaolab@gmail.com)

Materials Availability

Reagents generated in this study will be available upon request.

Data and Code Availability

This study did not generate dataset associated with the paper.

EXPERIMENTAL MODEL AND SUBJECT DETAILS

Mice

Gli1-LacZ (JAX#008211), *Gli1-Cre^{ERT2}* (JAX#007913), *Ai14* tdTomato reporter (JAX#007908), *β-Catenin$^{flox/flox}$* (JAX#004152), *Synapsin1-Cre* (JAX#003966), *Axin2-LacZ* (JAX#009120), *LepR-Cre* (JAX#008320), *NG2-Cre^{ERT}* (JAX #008538), and *Pdgfrα-Cre^{ER}* (JAX #018280) mice were purchased from the Jackson Laboratory. Samples of *αSMA-CreERT2* mice (Wendling et al., 2009)were kindly provided by Dr. Woo-Ping Ge at UT Southwestern Medical Center. *Cdh5-CreERT 2* (Sörensen et al., 2009) mice were kindly provided by Dr. Ralph Adams at the Max Planck Institute for Molecular Biomedicine. *Ctnnb1$^{flx(ex3)}$* (Harada et al., 1999) and *Sost-LacZ* (Collette et al., 2012) mice were housed at Texas A&M University, College of Dentistry. For all *in vivo* studies, sex- and age-matched littermate mice were used in control and experimental groups. No significant differences were detected between male and female mice. In most of our experiments, unless being specified, mice of 5-8 weeks of age were indicated as adult.

Animal Care and Use

Mice were housed in a temperature-controlled animal facility with a 12-hour light cycle. All mouse experiments were performed in accordance with the regulatory standards and all procedures were approved by the Animal Care and Use Committee of Texas A&M University, College of Dentistry.

METHODS DETAILS

Periodontium Cell Culture

Primary periodontium cells were isolated and cultured based on outgrowth method as previously described (Tran et al., 2014). Mandibles and maxilla of either male or female mice were dissected immediately after the mice were euthanized. Gingival tissue was removed to avoid gingival cell contamination. Intact molars were isolated under microscopy. Teeth explants were placed on culture dish for explant culture in DMEM low glucose supplemented with 10% FBS 2mM glutamate, 50U/mL penicillin and 50U/mL streptomycin, at 37°C in regular atmospheric conditions.

Tamoxifen Administration

Tamoxifen was dissolved in corn oil at 20 mg/ml as working solution. Unless being specified, mice were injected intraperitoneally at a dosage of 1.5mg/10g body weight for two consecutive days. This dosage was defined as the full dosage. The day of the first tamoxifen injection is defined as day 1.

For tamoxifen titer assay, titers of 1/16th n, 1/32th, 1/64th or 1/128th of the full dosage was injected to the mice intraperitonially once. Mice were euthanized on day 3 after the injection and lower first molars were collected and sectioned for imaging.

For *in vivo* colony tracing assay, 1/128th of full dosage (12μg/10g body weight) was injected to mice once. Mice were euthanized at indicated time points after induction and lower first molars were collected and sectioned for imaging.

Mice Perfusion and Sample Harvest

After anesthesia with Xylazine (110-12.5 mg/kg) and Ketamine (80–100mg/kg), mice were injected transcardially with 50mL 0.05M EDTA. Then 30mL 4%PFA was infused transcardially. Samples were dissected and fixed in 4%PFA overnight.

Mice PDL injury assay

Under anesthesia, maxillary or mandibular first molars on the experimental side of the mouth were punched with 28G needle at the furcation region. After surgery, mice were housed individually and provided with soft food. Tamoxifen was injected on day one and day two after surgery.

Immunofluorescent and GS-IB4 Staining

After fixation, samples were decalcified in 20% EDTA at 4°C for 1 week. Samples were embedded in OCT for frozen sectioning. 10μm sections were obtained. Sections were incubated with primary antibody at 4°C O/N. The following primary antibodies were used in this study: Anti-CD44, Anti-CD73, Anti-CD146, Anti-Periostin, Anti-Col I, Anti-Sp7, Anti-ß3-tublin, Anti-αSMA, Anti-LepR, Anti-ß-gal, Anti-SOST, Anti-Perilipin-1, Anti-CD31, Anti-CD34, and Anti-Nestin, Anti-NG2, Anti-PDGFRa, Anti-SHH. The secondary antibodies included goat anti-mouse (Invitrogen A11029, 1:100), anti-rat (Invitrogen A11006), anti-rabbit (Invitrogen A11034) IgG conjugated to Alexa 488, and goat anti-chicken IgY conjugated to AlexaFluo 488 (Abcam ab150169).

GS-IB4 (Isolectin GS-IB4 from Griffonia Simplicifolia) has been widely used for labeling endothelial cells in various organs including long bone marrow, lung, heart and retina (Epah et al., 2018; Hooper et al., 2009; Xu et al., 2018; Ohle et al., 2012; Arnold et al., 2012). For periodontium vasculature staining, mouse samples were fixed with 4% PFA overnight and decalcified in 20% EDTA for one week. Samples were embedded in OCT and 20μm sections were obtained. Sections were incubated with GS-IB4 conjugated with AlexaFluo488 (Invitrogen) at 1:100 dilution at 4°CC O/N. Sections were then briefly washed with PBS and counterstained with DAPI for imaging.

X-gal Staining

Samples were fixed in 0.2% glutaraldehyde at 4°C O/N and decalcified in 10% EDTA with 2 mM $MgCl_2$ at 4°C for 2 weeks. Samples were embedded in OCT for frozen sectioning. 10μm sections were obtained. After washing in ice-cold PBS with 2mM $MgCl_2$, sections were pre-fixed in ice-cold 4% PFA for 10min, then incubated in X-gal staining buffer (PBS with 2mM MgCl2, 0.01% Sodium deoxycholate, 0.02% Igepal, 6mM Potassium ferrocyanide(II), 6mM Potassium ferricyanide(III), 20nM Tris (PH 7.3)1mg/ml X-gal) at 37°C for 30 min - 8 hour until the blue pattern became clear. 0.1% Nuclear fast red solution and 0.05% Eosin Y solution were applied for counterstaining.

Long Duration EdU Incorporation Assay

Turnover of the PDL tissue is much slower than mouse hair follicle or incisor, which made it difficult to demonstrate dividing cells with conventional single-dose EdU incorporation assay within a 2- or 4- hour duration. Therefore, we gave multiple EdU injections (12hr interval) for mice in longer durations of 24hr, 48hr, 96hr or one week. Within each 24-hour cycle, three shots of EdU were given at 9am, 9pm and 9am/next day. Mice were euthanized two hours after the last injection.

In Figures S3 and S7, both tamoxifen induction and long term EdU incorporation assays were performed to label Gli1+ cells and dividing cells. Experiments were carefully scheduled to coordinate tamoxifen and EdU injection time.

For the 24hr EdU assays in Figures S3A, S7A, and S7D, tamoxifen was injected on day1 and day2. EdU was injected at 12-hr intervals on day 2 and day 3. On day 3, samples were collected twohours after the last EdU injection.

For the 48hr EdU assay in Figure S3B, tamoxifen was injected on day 1 and 2. EdU was injected at 12-hr intervals on day 1, 2 and 3. Samples were collected twohours after the last EdU injection.

For the 96hr and 1wk EdU assays in Figures S3C and S3D, EdU injections were first initiated at 12-hr intervals for 96hr or one week. Tamoxifen was injected at two days and one day (once per day) prior to the sample collection day to label Gli1+ cells. Samples were collected twohours after the last EdU injection.

In Figure S3E, adult mice were first induced with tamoxifen. Three weeks after induction, EdU was injected at 12-hr intervals for one week. Samples were collected twohours after the last EdU injection on day 30 after induction.

In Figures S3G and S3H, the injection schedule was displayed above the figure panel.

For each injection, EdU was given intraperitoneally at a dosage of 2 mg/10 g body weight. Horizontal sections of the mouse molars at mid-root position were acquired after processing. Invitrogen EdU detection kit was used to detect EdU following the manufacturer's protocol.

PEGASOS Tissue Clearing and 3D Image Acquisition

Tissue clearing with the PEGASOS method was performed as previously described (Jing et al., 2018). In brief, after perfusion, mouse mandibles were dissected and fixed in 4% PFA. Decalcification was carried out in 10% EDTA at 37°C for 1 week. Decolorization was carried out by shaking samples in 25% Quadrol (Sigma-Aldrich 122262) at 37°C for 2 days. Delipidation was performed in gradient 30%, 50% and 70% tert-butanol aqueous solutions (Sigma-Aldrich 360538) at 37°C. Dehydration treatment was performed with tB-PEG solution composed of 72% tert-butanol, 25% PEGMMA500 (Sigma-Aldrich 409529) and 3% Quadrol. For clearing, samples were immersed the BB-PEG clearing solution composed of 72% benzyl benzoate (Sigma-Aldrich 409529), 25% PEGMMA500 and 3% until complete transparency was achieved in about 24 hours. Samples were stored in the BB-PEG solution at room temperature for imaging. 3-D imaging was performed with a Zeiss upright LSM780 2-photon microscope. 3D image reconstruction was performed with Imaris 9.0.

Occlusal Force Unloading Experiment

One-month-old mice were used in a split-mouth design. In the *Sost*$^{-/-}$ mouse rescue experiment, one-month-old littermate mice of the same sex with different genotypes were assigned to the control and experimental groups. Under anesthesia, three maxillary or mandibular molars on the experimental side of the mouth were removed with fine needle and forceps. After surgery, mice were housed individually and soft food was provided. Tamoxifen induction was performed on day one and day two after the surgery. The unloading procedure had no significant impact on the food or water intake of the mice.

Real Time-PCR and Analysis

Qiagen RNeasy Mini Kit was used for total RNA extraction. Intact mouse molars were extracted immediately after sacrificing and placed in lysis buffer on ice immediately. Any broken teeth were discarded in order to prevent contamination with dental pulp. Extracted teeth were repeatedly pipetted with a 28 g syringe needle in lysis buffer on ice 20 times. Supernatant was used for the RNA extraction process based on the manufacturer's protocol. 5xAll-in-one 1st Strand cDNA Synthesis Mix was used to carry out reverse transcription. 2xqPCR Master Mix was used for real time PCR.

Gapdh was used as the internal control. ΔΔCt method was used for expression calculation. Relative expression was calculated by nomadized with mean of control group. A parametric unpaired two-tailed Student's test was carried out.

Periodontium Cells Differentiation Assay

Trilineage differentiation experiments were performed as previously described (Zhao et al., 2015). Osteogenic, chondrogenic and adipogenic differentiation induction media were prepared according to the manufacturer's protocols. For osteogenic differentiation, cells were seeded at 3 x 10^4 cells/well in a 24-well plate and differentiated in induction medium for 28 days, then fixed in 4% PFA and stained in 2% Alizarin Red solution. For adipogenic differentiation, cells were seeded at 3 x 10^4 cells/well in a 24-well plate and differentiated in induction medium for 28 days, then fixed in 4% PFA and stained in 0.5% Oil Red O solution. For adipogenic differentiation, 20 μL cell suspension was seeded in the center of wells of a 12-well culture plate at a density of 1 x 10^6 cells/ml. Four hours after cell attachment, induction medium was added. Cells were cultured for 28 days, then fixed in 4% PFA and stained in 1% Alcian Blue solution.

MicroCT Scanning and Analysis

After fixation, CT scans were performed with the μCT-35 system (Scanco Medical; 70-kV voltage, 7.0 μm, high resolution). ImageJ was used for format conversion from .ISO to .TIF. Imaris was used for 3D reconstruction and quantification.

Cementum Enamel Junction-Alveolar Bone Crest (CEJ-ABC) distance was measured at multiple sites per tooth (6 for 1st and 2nd molar, 4 for 3rd molar) in Imaris by calculating the distance between the CEJ and ABC in 3D view. Bone density was measured in Imaris by calculating the signal intensity in the ROI.

QUANTIFICATION AND STATISTICAL ANALYSIS

All experiments were performed at least three times and representative image were chosen for publication. Where appropriate, the number of experiments (individual mice or biological replicates) is given in figure or legend. All values are represented as mean ± SD. GraphPad Prism 8 was used for statistical analysis. NEJM formatting for P values was used (ns when no significance, * when $p<0.05$, ** when $p<0.01$, *** when $p<0.001$).

In the split-mouth design (Figures 6M, 6P, and S3I), paired control and experiment groups were from the same mouse. Values from sites of experimental side were normalized by dividing the values of corresponding sites from the control side. Then a parametric two-tailed *Student*'s *test* was carried out.

When control and experiment groups were from different mice (Figures 4S, 4T, 5F, 5K, S4O, S7G, S7H, and S7I), multiple values from different sites were normalized by dividing the mean value of the same site from the control group. Then the average of values

from each mouse was used as the final result of that mouse and a parametric unpaired two-tailed *Student*'s *test* was carried out. One-way ANOVA was carried out when more than two groups were compared (Figure S3F).

For quantification based on tissue slides, one slide per mice were used. In the region of interest (ROI), cells with tdTomato and DAPI co-staining were defined as positive cells, while cells with only DAPI signal were defined as negative cells. For quantification based on 3D tissue image, one 3D image stack (200μm X 200μm X 200μm voxel size) per mouse was used. Second harmonic generation (SHG) signal was used to outline the structure in 3D. In the ROI, the volume filled with tdTomato signal was defined as positive, while the volume without tdTomato was defined as negative. The volume size was measured with the Surface function within the Imaris 9.0 (Bitplane). The ratio of volume size was used to represent the percentage of positive cells.